frontiers | Frontiers in Chemistry

TYPE Original Research
PUBLISHED 21 September 2022
DOI 10.3389/fchem.2022.949205

OPEN ACCESS

EDITED BY
Pezhman Shiri,
Shiraz University of Medical Sciences, Iran

REVIEWED BY
Shahrzad Abdolmohammadi,
Islamic Azad University South Tehran Branch, Iran
Jasem Aboonajmi,
Shiraz University, Iran
Ramin Javahershenas,
Urmia University, Iran
Radomir Jasiński,
Cracow University of Technology, Poland
Atefeh Roosta,
Tianjin Institute of Industrial Biotechnology (CAS), China

*CORRESPONDENCE
Zinatossadat Hossaini,
zshossaini@yahoo.com

SPECIALTY SECTION
This article was submitted to Organic Chemistry, a section of the journal Frontiers in Chemistry

RECEIVED 20 May 2022
ACCEPTED 13 July 2022
PUBLISHED 21 September 2022

CITATION
Hossaini Z, Mohammadi M and Sheikholeslami-Farahani F (2022), Six-component synthesis and biological activity of novel spiropyridoindolepyrrolidine derivatives: A combined experimental and theoretical investigation. *Front. Chem.* 10:949205. doi: 10.3389/fchem.2022.949205

Six-component synthesis and biological activity of novel spiropyridoindolepyrrolidine derivatives: A combined experimental and theoretical investigation

Zinatossadat Hossaini[1]*, Marziyeh Mohammadi[2] and Fatemeh Sheikholeslami-Farahani[3]

[1]Department of Chemistry, Qaemshahr Branch, Islamic Azad University, Qaemshahr, Iran, [2]Department of Chemistry, Faculty of Science, Vali-e-Asr University of Rafsanjan, Rafsanjan, Iran, [3]Department of Chemistry, Firoozkooh Branch, Islamic Azad University, Firoozkooh, Iran

Petasites hybridus rhizome water extract was used as green media for the preparation of Ag/Fe_3O_4/CdO@multi-walled carbon nanotubes magnetic nanocomposites (Ag/Fe_3O_4/CdO@MWCNTs MNCs), and its activity was evaluated by using in the one-pot multicomponent reaction of isatins, acetyl chloride, secondary amines, vinilidene Meldrum's acid, primary amines, and malononitrile in an aqueous medium at room temperature for the generation of spiropyridoindolepyrrolidine as new derivatives with tremendous output. In addition, organic pollutant reduction of 4-nitrophenol (4-NP) was carried out by generated Ag/Fe_3O_4/CdO@MWCNTs in water at room temperature. The results displayed that Ag/Fe_3O_4/CdO@MWCNTs were reduced as pollutants of organic compounds in a short time. The synthesized spiropyridoindolepyrrolidine has an NH_2 functional group that has acidic hydrogen and shows high antioxidant ability. Also, the spiropyridoindolepyrrolidine exhibited antimicrobial ability, and the method that is used for this purpose is the disk diffusion method, and two kinds of bacteria, Gram-positive and Gram-negative, were employed for this analysis. Also, to better understand the reaction mechanism density, functional theory-based quantum chemical methods have been applied. For the generation of spiropyridoindolepyrrolidine, the used process has many properties such as reactions with short time, product with good yields, and simple extraction of catalyst from the mixture of reaction.

KEYWORDS

Ag/Fe 3 O 4 /CdO@MWCNTs, vinilidene Meldrum's acid, acetyl chloride spiropyridoindolepyrrolidine, six component reactions, isatins

1 Introduction

Among organic compounds, heterocyclic organic compounds are important because of their application in medicinal chemistry and show many biological activities (Goel et al., 2004; Amir et al., 2007; Abdolmohammadi, et al., 2010; Siddiqui, et al., 2011; Lamberth and Dinges, 2012; Abdolmohammadi, 2013; Abdolmohammadi, et al., 2013; Abdolmohammadi, 2014a; Lashkari, et al., 2015; Martins, et al., 2015; Desai et al., 2016; Zhao et al., 2017; Fouad et al., 2018; Kalaria et al., 2018; Khattab and Rehan 2018; Li et al., 2018; Sokolova et al., 2018; Zhao et al., 2019; Aboonajmi, et al., 2021). Thus, due to the importance of these compounds, many procedures were reported for the synthesis of heterocyclic compounds. One of the most important procedures for the synthesis of these compounds with biological activity is multicomponent reactions (MCRs) (Ibarra, et al., 2018; Zhi et al., 2019). MCRs are significant because they have benefits such as atom economic and synthesis of high-yield heterocyclic compounds in comparison to other procedures (Tietze et al., 2006; Weber, et al., 1999; Herrera and Marqués-López, 2015). Multicomponent reactions (MCRs) are considered to be an important methodological arsenal in synthetic and medicinal chemistry. These reactions have been strategically employed in various synthetic transformations where classical methods usually involve many steps with tedious procedures. The MCR approach provides high yields, atom-/step economy, reduced reaction time, is ecofriendly, and acts as an amenable tool for the generation of a library of new chemical entities (NCEs), especially in the drug discovery process. Extensive research has led to copious developments in the field of MCRs. The developments have emerged with different synthetic approaches, including C–H activation, coupling, and cycloaddition, and eventually, such an amalgamation has enabled access to a broad spectrum of organic frameworks. Some of the procedures for the synthesis of heterocyclic compounds employed the catalyst for performing the reactions. The transition metal oxide nanostructures with high active surface area could be used as catalysts in these reactions. Also, these catalysts are employed in technology and applied science (Sahay et al., 2012; Yang et al., 2019; Zhao et al., 2019; Chen et al., 2020; Yang et al., 2020). MWCNTs, owing to large surface area and high adsorption capability, have been extensively investigated (Zhang, et al., 2013; Khalilian et al., 2017; Samani et al., 2018;

Synthesis of Novel Spiropyridoindolepyrrolidine

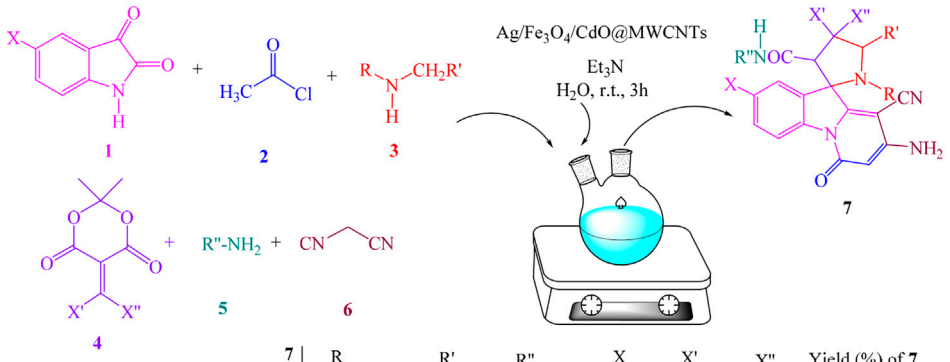

7	R	R'	R''	X	X'	X''	Yield (%) of 7
a	Me	H	Me	H	Me	Me	95
b	Et	Me	Et	H	Me	Me	90
c	$CH(Me)_2$	Me_2	Me	H	Me	Me	90
d	$CH(Me)_2$	Me_2	Et	H	Me	Me	87
e	Me	H	Et	H	Me	H	87
f	Me	H	Me	H	Me	H	95
g	Me	H	Me	H	Ph	H	90
h	Me	H	4-OMe-Bn	H	Me	H	85
i	$4\text{-}NO_2\text{-}C_6H_4$	Me	Me	H	Me	Me	75
j	$4\text{-Me-}C_6H_4$	H	Me	H	Me	Me	80
k	Me	H	Me	Me	Me	Et	75
l	Me	H	Ph	Me	Me	Me	85

SCHEME 1
Synthesis of spiropyridoindolepyrrolidines **7**.

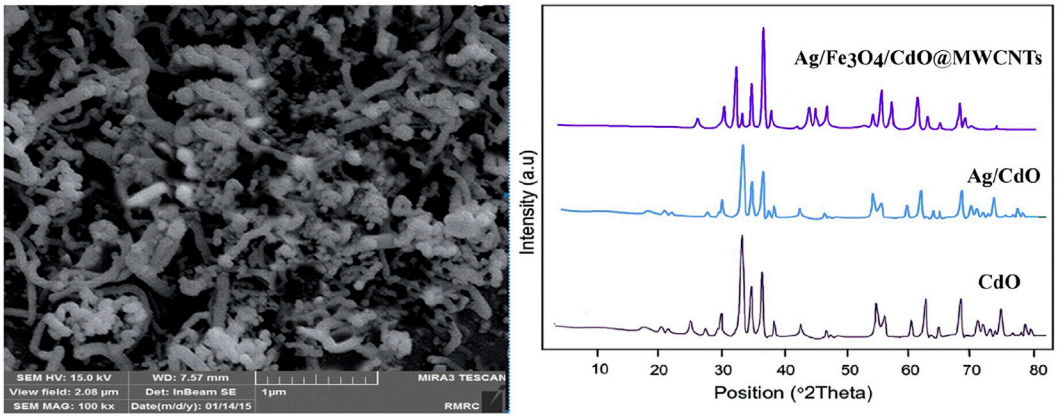

FIGURE 1
Left: SEM image of Ag/Fe_3O_4/CdO@MWCNT MNCs. Right: the XRD analysis of Ag/Fe_3O_4/CdO@MWCNT MNCs.

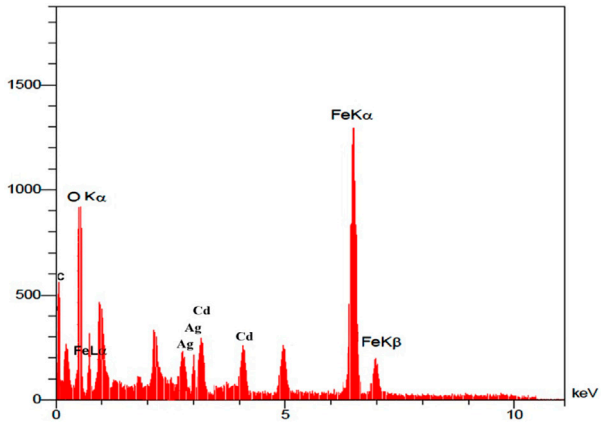

FIGURE 2
EDX image of Ag/Fe_3O_4/CdO@MWCNT MNCs.

Abdolmohammadi, 2018; Abdolmohammadi et al., 2019; Abdolmohammadi et al., 2020b). In the recent past, the supported catalyst and bimetallic oxide or trimetallic oxide catalysts were significant due to their high potentials in carrying out highly selective and efficient organic reactions (Guo et al., 2004; Wachs, 2005; Dastan et al., 2012; Rabiei, et al., 2017; Fakheri-Vayeghan, et al., 2018; Janitabar-Darzi and Abdolmohammadi, 2019; Chaghari-Farahani, et al., 2020; Abdolmohammadi, et al., 2022; Zare Davijani et al., 2022a). Metal oxides have high-crystalline structure and catalytic efficiency (Shi, 2013; Mousavi, et al., 2014; Jabłonska and Palkovits, 2016; Sharghi, et al., 2018). For this reason, the mixture of two or more metals and their curing procedures permit the change of the properties of materials' surface and optimization of the properties for a particular goal (Zhang et al., 2012; Lin-Bing et al., 2015). Therefore, the mixture of metal oxide catalysts and nanocomposite structures of them exhibited production of heterocyclic compounds according to green rules with high efficiency (Abdolmohammadi, et al., 2019; Abdolmohammadi et al., 2020a; Kalantari et al., 2020; Abdolmohammadi, et al., 2021; Khalilzadeh et al., 2021). Among the metal oxide nanoparticles, Fe_3O_4 magnetic nanoparticles (MNPs) are important because of high surface area, simple removing from reaction, and employment of it in MCRs several times. Another subject that is investigated in this research is the study of biological abilities such as the antioxidant and antimicrobial activity of synthesized spiropyridoindolepyrrolidines. Compounds with antioxidant activity could eliminate the negative effect of free radicals due to having reduction chemical structure. Also, these compounds could be employed as transitional metals chelators, and many sicknesses could be decreased or treated by these compounds (Halliwell, 1999; Liu and Meydani, 2002; Babizhayev et al., 2004; Djurišić et al., 2012). Another investigation of biological activity is the antimicrobial ability of synthesized compounds. Some of the bacteria do not get killed by utilizing drugs, and these bacteria cause many diseases in humans and animals. For this reason, finding out good yielding procedures for decreasing this problem and investigation of the antimicrobial properties of synthesized compounds are important. Dyes and pigments are two important subjects that are used in the generation processes of food, drug, textile, and printing. The production of dyes and pigments is about ~7 × 105 tons in one year, and these are very unsafe and dangerous for aquatic system organisms (Kassaee, et al., 2004; Yavari, et al., 2007; Yavari et al., 2010; Ezzatzadeh and Hossaini 2019). For this reason, discovering green and eco-friendly procedures for removing dye and pigment pollutants from the environment is very important. Many of these procedures that are investigated in the literature produced a byproduct, and for

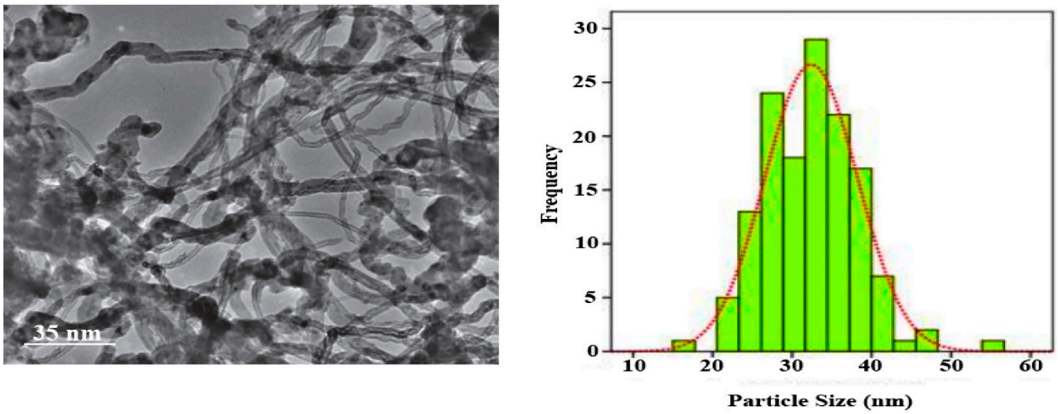

FIGURE 3
TEM image and histogram curve of Ag/Fe_3O_4/CdO@MWCNT MNCs.

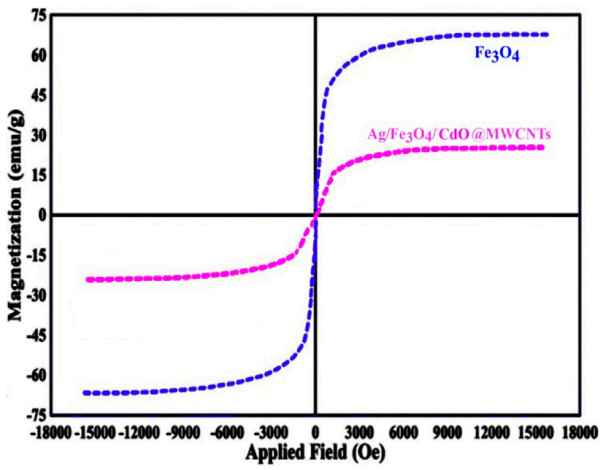

FIGURE 4
VSM analysis of the green Ag/Fe_3O_4/CdO@MWCNT MNCs.

this reason, they are not suitable for usage. Also, recently, the application of nanotechnology in water treatment has gained wide attention and is being actively investigated due to its remarkable properties (Kassaee et al., 2008; Sabbaghan et al., 2010; Rustaiyan and Ezzatzadeh, 2011; Ezzatzadeh et al., 2012; Shahvelayati and Esmaeeli, 2012; Zhang et al., 2013; Salehi Borban et al., 2017; Shahvelayati et al., 2017; Seifi Mansour et al., 2019; Ghambarian et al., 2020; Ghashghaee and Ghambarian, 2020; Shafaei et al., 2020). In the field of water treatment, nanotechnology can be classified into three main applications: 1) to restore (remediate) and purify contaminated water, 2) to detect pollution, and 3) to prevent pollution. This has led to the demand for nanosensors with high sensitivity for the detection of micro-, nano-, and molecular pollutants. Therefore, high-efficiency methods or actively synthesized compounds were needed for eliminating or decreasing these problems. In recent years, we studied about enhancing new and easy processes for the generation of important heterocyclic compounds (Babizhayev et al., 2004; Ebrahimi, et al., 2008; Kassaee et al., 2010; Yavari et al., 2010; Khandan-Barani et al., 2011; Rustaiyan, et al., 2011; Rustaiyan, et al., 2011; Shahvelayati et al., 2012; Ezzatzadeh et al., 2012; Hassanabadi and Khandan-Barani, 2013; Masoodi, et al., 2013; Abdolmohammadi, 2014b; Maghsoodlou, et al., 2014; Azizi et al., 2015; Hajinasiri et al., 2015; Khandan-Barani et al., 2015; Balar et al., 2016; Balar et al., 2016; Ghambarian et al., 2016; Soleimani Amiri, et al., 2016; Ghambarian et al., 2017; Koohi, et al., 2017; Salehi Borban et al., 2017; Shahvelayati et al., 2017; Soleimani-Amiri et al., 2018; Abdolmohammadi and Hossaini, 2019; Ghashghaee et al., 2019; Hekmatara et al., 2019; Mohammadi, et al., 2019; Seifi Mansour et al., 2019; Abdolmohammadi et al., 2020a; Ghashghaee et al., 2020a; Ghashghaee et al., 2020b; Shafaei et al., 2020; Ghavidel, et al., 2021; Zare Davijani et al., 2022b). In this research, initially, a green procedure was employed for the generation of new spiropyridoindolepyrrolidines **7** *via* MCRs of isatins **1**, acetyl chloride **2**, secondary amines **3**, vinilidene Meldrum's acid **4**, primary amines **5,** and malononitrile **6** in an aqueous medium at room temperature in the vicinity of Ag/Fe_3O_4/CdO@MWCNT MNCs as an organometallic catalyst in aqueous media at room temperature (Scheme 1).

2 Results and discussion

In this study, the new spiropyridoindolepyrrolidines **7** have been produced with excellent efficiency employing six component reactions of isatins **1**, acetyl chloride **2**, secondary amines **3**, vinilidene Meldrum's acid **4**, primary amines **5,** and

TABLE 1 Determination of the best conditions such as the catalyst, amount of catalyst, and temperature for the synthesis of 7a.

Entry	Catalyst	Temp. (°C)	Catalyst (g)	Time (h)	Yield %[a]
1	None	r.t	-	10	-
2	None	100	-	8	-
3	CdO-NPs	r.t	0.01	4	45
4	CdO-NPs	r.t	0.015	3	58
5	CdO-NPs	r.t	0.02	3	65
6	Fe_3O_4-MNPs	r.t	0.015	3	35
7	Ag NPs	r.t	0.015	3	78
8	MWCNT	r.t	0.015	3	27
9	CuO-NPs	r.t	0.015	3	38
10	Ag/Fe_3O_4/CdO	r.t	0.015	3	80
11	Fe_3O_4/CdO	r.t	0.015	3	70
12	Ag/CdO@ MWCNT	r.t	0.015	3	78
13	Fe_3O_4/CdO/MWCNT	r.t	0.015	3	70
14	CdO@ MWCNT	r.t	0.015	3	68
15	Ag/Fe_3O_4/MWCNT	r.t	0.015	3	75
16	Ag/Fe_3O_4/CdO@MWCNT	r.t	0.015	3	87
17	**Ag/Fe_3O_4/CdO@MWCNT**	**r.t**	**0.02**	**3**	**95**
18	Ag/Fe_3O_4/CdO@MWCNT	reflux	0.02	3	95
18	Ag/Fe_3O_4/CdO@MWCNT	r.t	0.015	3	87
19	Ag/Fe_3O_4/CdO@MWCNT	r.t	0.025	3	95

[a]Isolated yields. Bold indicates best condition for performing reactions.

TABLE 2 Determination of the best solvent for the generation of 7a.

Entry	Solvent	Time (h)	Yield %[a]
1	EtOH	15	None
2	CH_2Cl_2	8	60
3	$CHCl_3$	5	68
4	**H_2O**	**3**	**95**
5	Solvent free	8	58
6	DMF	12	30
7	Toluene	12	68
8	CH_3CN	5	90

[a]Isolated yields.
Bold indicates best condition for performing reactions.

TABLE 3 Number of reusability of the catalyst for the synthesis of compound 7a.

Run	% yield[a]
1st	95
2nd	95
3rd	92
4th	90
5th	87

[a]Isolated yields.

malononitrile **6** in aqueous media at room temperature in the vicinity of Ag/Fe_3O_4/CdO@MWCNT MNCs as a new reusable organometallic nanocatalyst. The water extract of *Petasites hybridus* rhizome was used for the preparation of Ag/Fe_3O_4/CdO@MWCNT MNCs, and for the confirmation of the prepared catalyst structure, scanning electron microscopy (SEM) (Figure 1 (left)) and X-ray diffraction (XRD) (Figure 1 (right)) were employed. The SEM image of Ag/Fe_3O_4/CdO@MWCNT MNCs was used for the investigation and confirmation of the skeleton of the organometallic nanocomposite. The morphology, surface uniformity, and size of particles can be investigated by SEM analysis. The SEM images of Ag/Fe_3O_4/CdO and Ag/Fe_3O_4/CdO@MWCNT magnetic nanocomposites are shown in Figure 1 (left). Based on the FE-SEM images, Ag/Fe_3O_4/CdO MNCs have a spherical morphology, which is confirmed by the good dispersion of nanoparticles in the structure.

Another analysis for the confirmation of the structure of the nanocatalyst is X-ray diffraction (XRD) which was utilized for measuring the size of synthesized Ag/Fe_3O_4/CdO@MWCNT MNCs (Figure 1 (right)). All of the observed peaks at 2θ = 35.0, 44.0, 54.2, 57.2, and 63.0° can be contributed to Fe_3O_4 (JCPDS No. 19-629) that have the face-centered cubic phase. All peaks are for the pure Fe_3O_4, and the structure of Fe_3O_4 did not display any impurity. In the XRD analysis of synthesized Ag/Fe_3O_4/CdO@MWCNT, MNCs showed peaks at 2θ = 33.9, 54.8, and 68.2° that could be

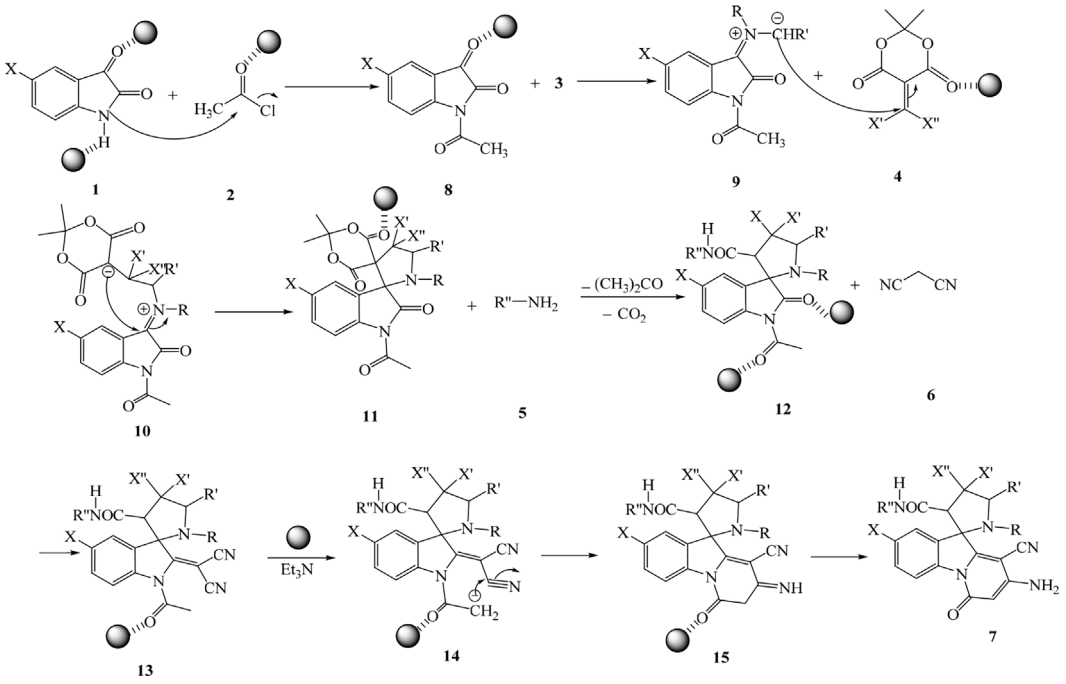

SCHEME 2
Proposed mechanism for the preparation of **7**.

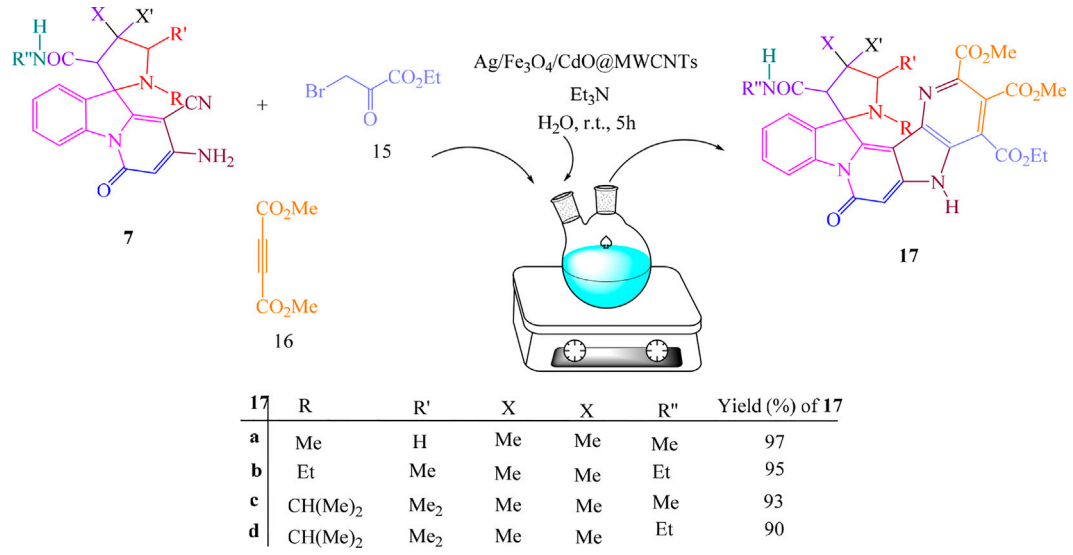

17	R	R'	X	X	R"	Yield (%) of **17**
a	Me	H	Me	Me	Me	97
b	Et	Me	Me	Me	Et	95
c	$CH(Me)_2$	Me_2	Me	Me	Me	93
d	$CH(Me)_2$	Me_2	Me	Me	Et	90

SCHEME 3
Synthesis of spiropyridines **17**.

contributed to (111), (311), and (222) planes and show the cubic construction for CdO moiety (JCPDS No: 73-2,245). The peaks in the XRD analysis of the synthesized catalyst that are attributed to Ag NPs are at 37.9, 44.6, 64.6, and 77.7° and (111), (200), (220), and (311) planes of Ag (JCPDS, No.04-0783), respectively, and the Ag_2O peak was not seen in XRD analysis. The typical peaks of MWNTs

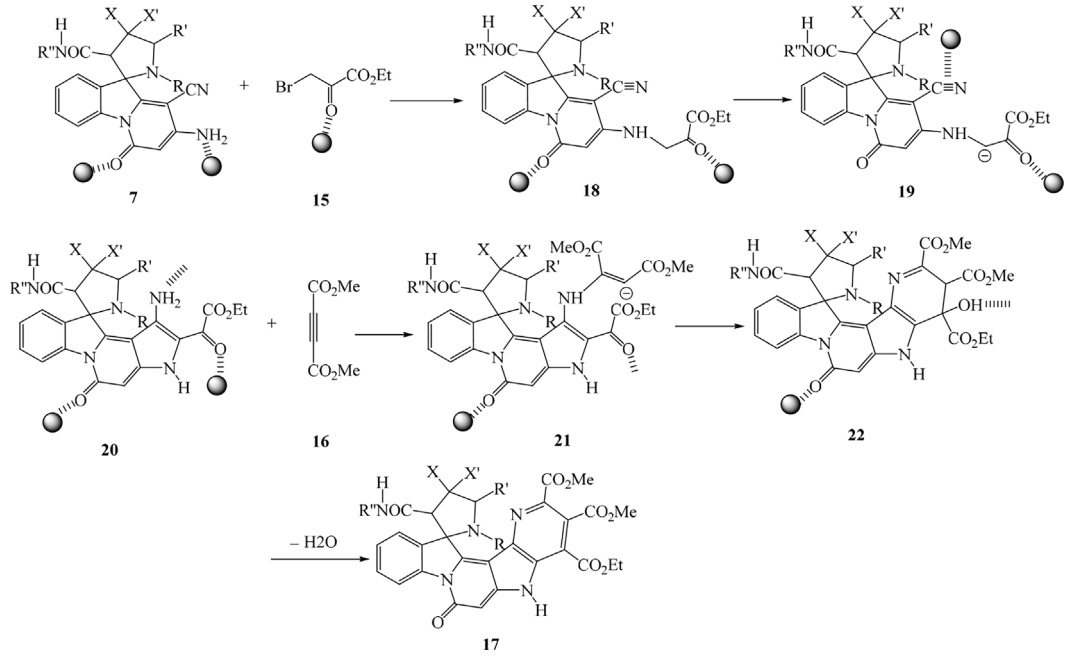

SCHEME 4
Proposed mechanism for the preparation of 17.

moiety (JCPDS No. 41-1,487) were seen as broad peaks around 26.2 and 43.6°.

The elemental analysis of the synthesized nanocatalyst was specified by the Energy Dispersive X-Ray Analysis (EDX) procedure (Figure 2). The peaks that are seen in the EDX analysis of $Ag/Fe_3O_4/CdO@MWCNT$ are Ag, Cd, Fe, O, and C peaks which confirmed the production of nanocatalysts. Additionally, the existence of peak of carbon confirmed that the organic compounds and multi-walled carbon nanotubes (MWCNTs) exist in the synthesized nanocatalyst.

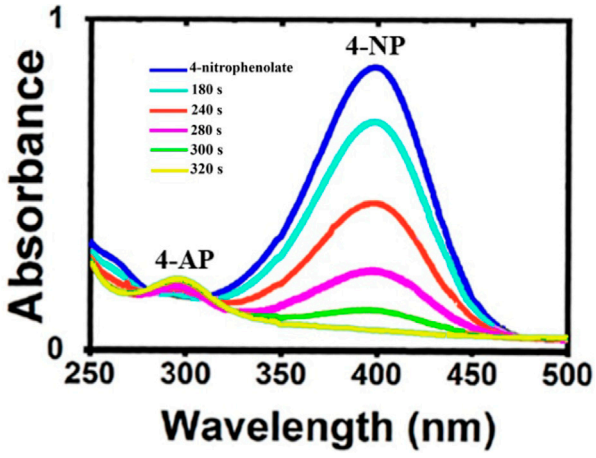

FIGURE 5
Reduction of the 4-NP to 4-AP by UV–Vis analysis.

In another technique for confirming the morphology of the $Ag/Fe_3O_4/CdO@MWCNT$, MNCs were considered by transmission electron microscopy (TEM) (Figure 3). Figure 3 (left) gives the TEM micrographs of clean $Ag/Fe_3O_4/CdO@MWCNTs$, and Figure 3 (right) gives the histogram curve of $Ag/Fe_3O_4/CdO@MWCNT$ MNCs.

To determine the mean size of the $Ag/Fe_3O_4/CdO@MWCNTs$ nanoparticles, we obtained the histogram (by measuring about 100 randomly chosen particles in the magnified TEM image) of the particle size distribution of $Ag/Fe_3O_4/CdO@MWCNTs$ (Figure 3 (right)). The graphical results in this figure show that the size of the $Ag/Fe_3O_4/CdO@MWCNT$ nanoparticles is in the range of 10–60 nm with the average particle size of 33 nm. The magnetic property of the synthesized nanocatalyst and pure Fe_3O_4 NPs was confirmed by measuring the value of saturation magnetization (VSM) Figure 4. According to the VSM analysis of nanocatalyst, the $Ag/Fe_3O_4/CdO@MWCNT$ MNCs' and pure Fe_3O_4 NPs' saturation magnetization is 28.3 emu/g and 67.5 emu/g, respectively (Figure 4). Because of the catalyst structure and coating effect of the synthesized catalyst, the magnetic response was decreased. The magnetic property of the synthesized catalyst caused easy separation of the catalyst from the aqueous solution.

We also evaluated the catalytic activities of the $Ag/Fe_3O_4/CdO@MWCNT$ MNCs through the synthesis of

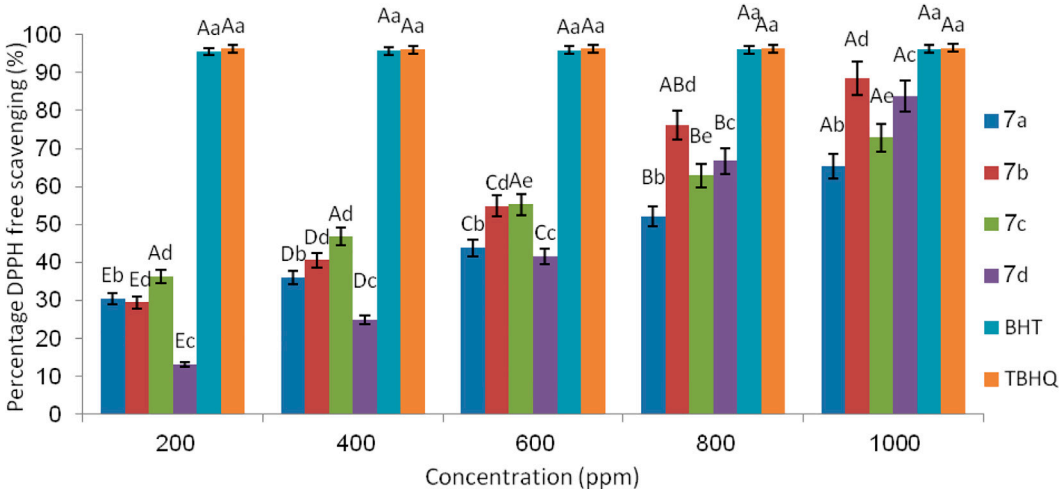

FIGURE 6
Order of antioxidant activity of **7a-7d** using DPPH.

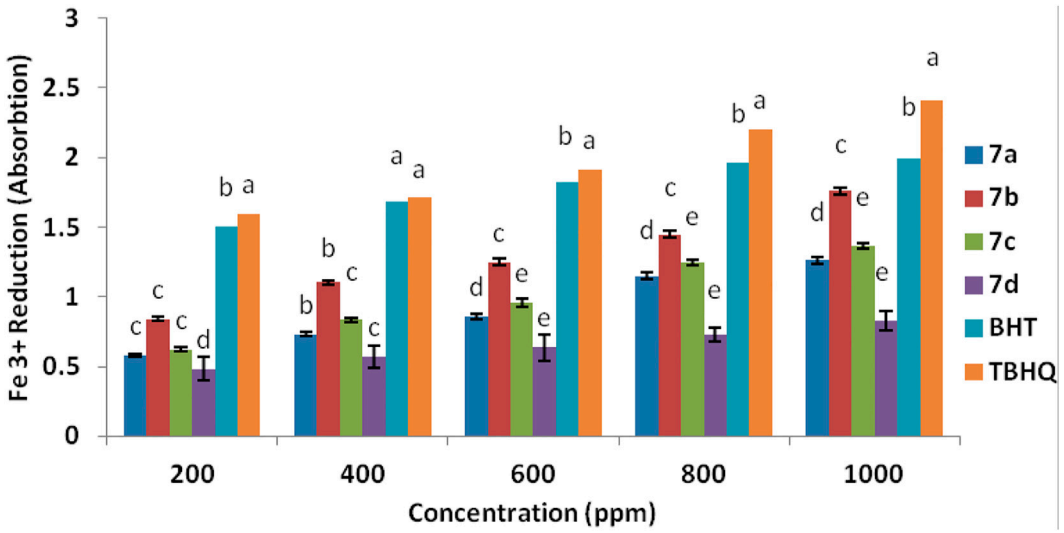

FIGURE 7
Ferric ions (Fe^{3+}) reducing antioxidant power (FRAP) of compounds **7a-7d**.

spiropyridoindolepyrrolidine derivatives in the presence of Ag/Fe_3O_4/CdO@MWCNT MNCs. The imperative subject in all organic reactions is obtaining the most excellent state for carrying out the reactions. In the beginning, for obtaining this goal, the multicomponent reaction of isatins **1a**, acetyl chloride **2**, dimethyl amine **3a**, isopropylene Meldrum's acid **4a**, methyl amine **5a,** and malononitrile **6** was chosen as a model reaction (Table 1). Without a catalyst, even after 10 h, the production of compound **7a** was not carried out (entry 1, Table 1). For optimizing the temperature of sample reaction and achieving the best temperature, the reaction temperature was enhanced to 100°C but did not exhibit significant variation in the efficiency of spiropyridoindolepyrrolidine **7a** (entry 2, Table 1). Also, these reactions were not carried out without a catalyst. For confirmation of this point, to the reaction mixture, CdO-NPs (0.01 g) were added as catalysts. After 4 h, spiropyridoindolepyrrolidine **7a** was generated in good efficiency (entry 4, Table 1). As a result, these reactions needed a catalyst for performing. For finding out the best catalyst for the model reaction, we considered a number of

TABLE 4 Antibacterial activity of spiropyridoindolepyrrolidines 7a-7g.

Compound	*Staphylococcus aureus* (+)	*Bacillus cereus* (+)	*Escherichia coli* (-)	*Klebsiella pneumoniae* (-)
7a	9	11	10	8
7b	**18**	**21**	**22**	**19**
7c	**17**	**21**	**22**	**18**
7d	10	7	11	8
7e	**17**	**19**	**20**	**22**
7f	10	9	11	12
7g	**19**	**23**	**24**	**22**
Streptomycin	18	24	25	23
Gentamicin	21	23	24	21

Bold indicates best condition for performing reactions.

nanocatalysts such as Ag NPs, Fe_3O_4 MNPs, CdO NPs, Fe_3O_4/CdO NPs, Fe_3O_4/CdO/MWCNTs, Ag@MWCNTs, MWCNTs, Ag NPs, and Ag/Fe_3O_4/CdO@MWCNTs. Among these catalysts, Ag/Fe_3O_4/CdO@MWCNTs are selected as nanocatalysts for the synthesis of spiropyridoindolepyrrolidine **7a,** and the product efficiency was increased by this catalyst. The Ag/Fe_3O_4/CdO@MWCNTs as catalysts have two sites in their structure. The three sites in the synthesized catalyst (Ag, Fe, and Cd) are Lewis acids and caused the activation of carbonyl groups. According to the results in Table 1, the Ag NPs are more useful than Fe_3O_4, CdO, Fe_3O_4/CdO, and Fe_3O_4/CdO/MWCNT. Ag is a stronger Lewis acid than Fe_3O_4 and TiO_2 and is very significant when these reactions were performed with catalytic amounts of Ag/Fe_3O_4/CdO/MWCNTs-MNCs. Therefore, as a result, increasing the Ag/Fe_3O_4/CdO/MWCNTs-MNCs' amount from 0.02 to 0.03 g did not illustrate any remarkable variation in the efficiency of the reaction. So, 0.02 g of Ag/Fe_3O_4/CdO/MWCNTs-MNCs was needed for the preparation of spiropyridoindolepyrrolidine with high efficiency (entry 11, Table 1), and the yield of compound **7a** is 95% after 3 h (entry 11, Table 1). The roles of nanocatalysts in the preparation of spiropyridoindolepyrrolidine derivatives are Lewis acid and Lewis base. Ag, Cd, and Fe as Lewis acid activate the carbonyl group for nucleophilic attack. As displayed in Table 1, among Lewis acids, Ag is more effective than Cd and Fe.

Because of the easy and simple extraction of Fe_3O_4 magnetic nanoparticles (MNPs) from the reaction mixture, employing it in several reactions is very significant. Additionally, another study in this research work is the investigation of solvents' effects that were investigated on the synthesis of compound **7a** in the presence of Ag/Fe_3O_4/CdO@MWCNT (0.02 g). The results in Table 2 display that for carrying out the reaction, water is the best solvent.

As illustrated in Table 1 and Table 2, Ag/Fe_3O_4/CdO@MWCNT-MNC (0.02 g) as an organometallic catalyst, room temperature, and aqueous media are the suitable conditions for the generation of spiropyridoindolpyrrolidine **7**. The reuse of the synthesized catalyst is an important factor in the synthesis of organic compounds. In this research, the synthesized nanocatalyst was reused five times for the synthesis of spiropyridoindolepyrrolidines **7a** (Table 3). The obtained results proved that the catalyst can be reused five times without any considerable change in its power (Table 3). For reusing magnetic nanocatalysts, the external magnet was needed for the separation of the catalyst from the reaction mixture. After separation, the catalyst was washed with water and dried at room temperature for 24 h and used again.

After each run for the synthesis of compound **7a**, the catalyst was removed from the reaction mixture, washed, and used again. For this reason, compound **7a** yield was reduced after five times due to the decrease in the amount of catalyst and separation of it after each run. It should be mentioned that after separation of the catalyst, the amount of catalyst maybe changed but the form and size of it were not altered after separation. The decrease in the amount of catalyst has the highest effect on the efficiency of compound **7a**. For confirming the structure of synthesized spiropyridoindolepyrrolidines **7**, ^{1}H NMR, ^{13}C NMR, IR, elemental analysis, and mass spectrum were employed. At 1.05 and 1.12 ppm in the ^{1}H NMR spectra of spiropyridoindolpyrrolidine **7a** were displayed two singlets for methyl protons. There were two singlets at 2.25 and 2.76 ppm for NMe protons, one singlet at 3.64 for CH proton, one singlet at 9.87 for NH and at 10.23 for NH_2 protons, and several signals for aromatic protons. The carbonyl moiety displays two resonances in the ^{13}C NMR spectra of **7a** at 164.8 and 173.5 ppm. Also, another route for confirming the existence of carbonyl groups in the construction of synthesized compounds is the IR spectrum. The preparation mechanism for the synthesized compounds **7** is shown in Scheme 2 (Sabbaghan, et al., 2010).

First, isatins **1** and acetyl chloride **2** react at room temperature in the presence of Ag/Fe_3O_4/CdO@MWCNT MNCs and intermediate **8** was generated. The secondary amines **3** react with the carbonyl group of intermediate **8** and

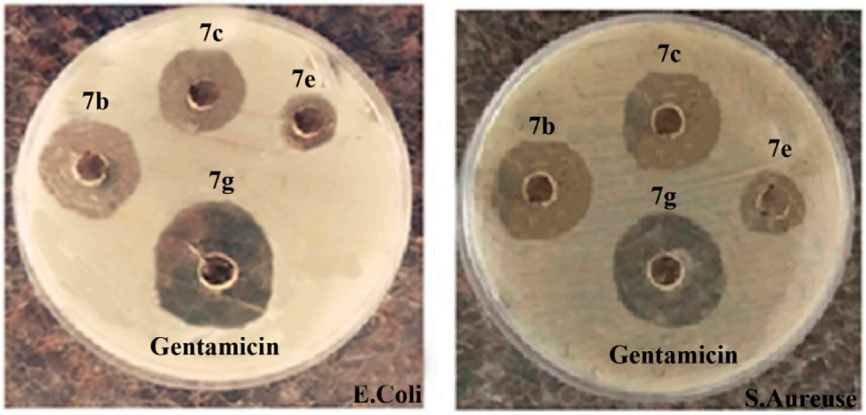

FIGURE 8
Comparison between the activity of the synthesized compounds with gentamicin.

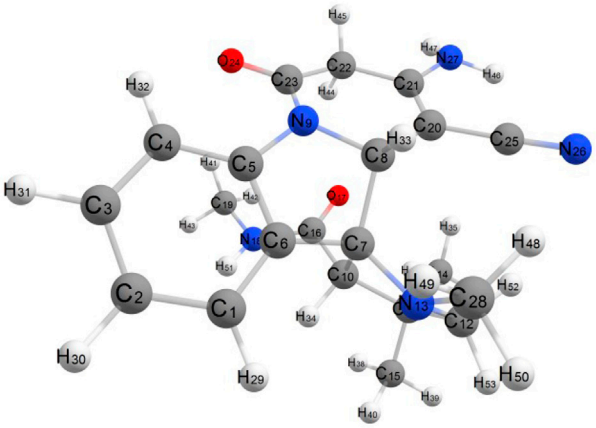

FIGURE 9
Optimized molecular structure.

produced the iminium ion **9** that with react with vinilidene Meldrum's acid **4** and produced intermediate **10**. Intermolecular cyclization of intermediate **10** produced intermediate **11** that was reacted with amines **5** and generated compounds **12** by the elimination of acetone and carbon dioxide. Compounds **12** react with malononitrile in the presence of catalyst and with intermolecular cyclization produced spiropyridoindolepyrrolidines **7**.

Under similar conditions and for confirming the structure of compounds **7**, the multicomponent reactions of spiropyridoindolepyrrolidines **7**, ethyl bromopyruvate **15,** and dimethyl acetylenedicarboxylate **16** in the vicinity of Ag/Fe_3O_4/CdO@MWCNT MNCs as an organometallic catalyst were performed in aqueous media at room temperature and produced spiropyridines 17 (Scheme 3).

For confirming the structure of compounds IR, ^{1}H NMR, and ^{13}C NMR, mass spectra were employed. At 1.05 and 1.10 ppm in the ^{1}H NMR of spiropyrrolopyridine **17a,** two singlets were displayed for methyl protons. The singlet at 2.76 related to NMe protons, the singlet at 3.07 attributed to CH_2 protons, and also, the singlets in the 3.61, 3.84, and 3.91 attributed to CH and two methoxy protons. One singlet at 5.15 ppm is for CH protone, and two singlets at 7.52 and 11.34 are for NH protones with aromatic protons resonances. The resonances at δ 165.2, 166.6, 168.8, and 172.1 ppm were contributed to four carbonyl groups of **17a**. Also, the carbonyl moiety in the structure of **17a** was confirmed by giving the IR spectrum**.** The proposed mechanism was recommended for the synthesis of compounds **17** as in Scheme 4.

Newly synthesized organometallic catalyst promoted the reduction of the organic pollutant

Another subject in this research is the investigation of the organometallic nanocatalyst effect on the elimination of the organic pollutant such as 4-nitrophenol. The effect of prepared Ag/Fe_3O_4/CdO@MWCNT MNCs on the reduction of 4-NP as a high-performance organometallic catalyst was studied in water at room temperature. The dye reduction processes were confirmed by giving the UV–Vis spectrum from the reaction mixture at ambient temperature. The reduction of 4-NP was not performed in the absence of the catalyst and $NaBH_4$ and did not display significant consideration. Therefore, Ag/Fe_3O_4/CdO@MWCNT MNCs were needed for the reduction of 4-NP to 4-aminophenol. The variation of reaction conditions monitored by UV–Vis analysis is exhibited in Figure 5. In the UV–Vis spectrum, the peak at 317 nm was contributed to the absorption of 4-nitrophenol in

10.3389/fchem.2022.949205

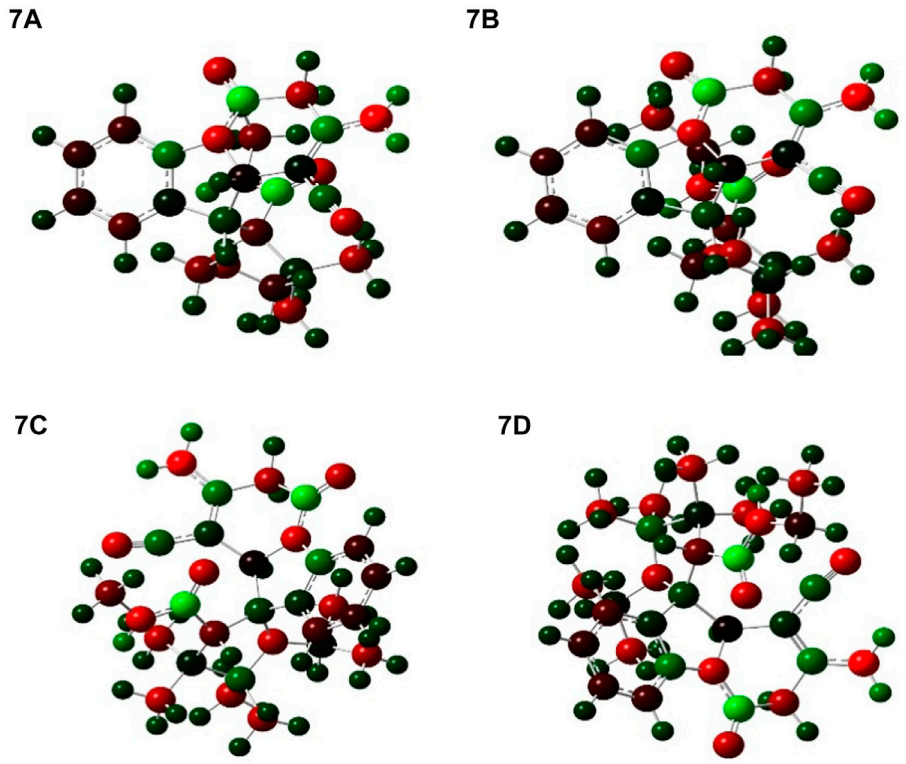

FIGURE 10
Distribution of Mulliken atomic charge for **7a-7d**.

TABLE 5 Mulliken atomic charges.

	Mulliken			
	7a	**7b**	**7c**	**7d**
C5	0.324458	0.327437	0.323153	0.320172
C8	−0.050852	−0.066118	−0.046142	−0.036001
C16	0.630508	0.665529	0.640289	0.639226
C19	−0.319524	−0.092239	−0.308651	−0.114158
C20	0.051492	0.133949	0.126907	0.121522
C21	0.388736	0.355951	0.321644	0.323730
C23	0.613744	0.596007	0.589181	0.592075

water, but when 4-nitrophenol converted to 4-nitrophenolate ion, the peak at 317 nm shifted to 400 nm as a red shift. After adding the newly prepared aqueous solution of $NaBH_4$, the color changed from yellow to colorless. If the solution was not added to Ag/Fe_3O_4/CdO@MWCNTs, the peak that was seen at 400 nm was not altered even after 15 h, which confirmed that reduction of 4-NP was not carried out in the absence of catalyst Ag/Fe_3O_4/CdO@MWCNTs with $NaBH_4$ and vice versa. When Ag/Fe_3O_4/CdO@MWCNTs were in 4-nitrophenol solution without $NaBH_4$, any considerable change in the color was not seen. For the elimination of the organic pollutant, the prepared organometallic nanocatalyst and $NaBH_4$ were needed, and in the presence of the catalyst and reducing agent, the peak of

TABLE 6 Energies, band gap, dipole moment (Debye), and electronegativity.

Compounds	Energy (eV)	E_{LUMO} (eV)	E_{HOMO} (eV)	Eg (eV)	Gap (Ev)	D (Debye)	χ
7a	-33728.55	-0.01926	-0.20271	0.18345	4.992	2.75	3.02
7b	-36937.873	-0.01656	-0.19743	0.18087	4.922	2.97	2.91
7c	-38006.657	-0.02117	-0.19908	0.17791	4.841	3.86	3.00
7d	-39076.357	-0.02077	-0.20295	0.18218	4.957	3.53	3.04

TABLE 7 Molecular descriptor results.

Compound	μ	η	S	ω	I	A
7a	−3.020	2.496	0.401	7.309	4.99	5.52
7b	−2.912	2.461	0.406	6.889	4.92	5.37
7c	−2.997	2.421	0.413	7.420	4.84	5.42
7d	−3.044	2.479	0.403	7.476	4.96	5.52

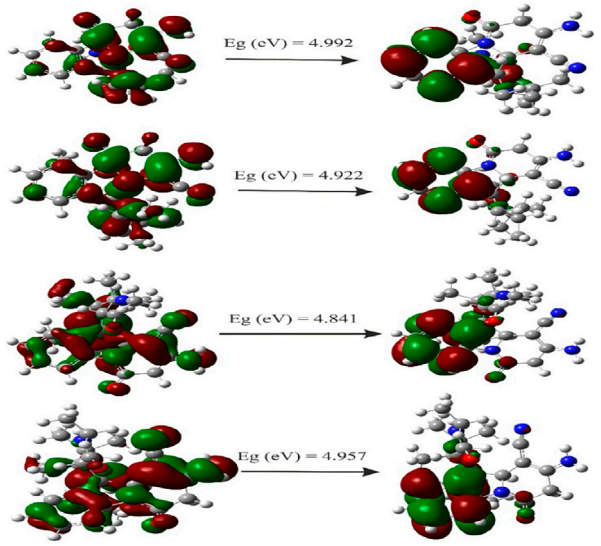

FIGURE 11
Plot HOMO and LUMO orbitals for 7a–7d compounds.

absorbance at 400 nm quickly within 5 min reduced to about zero. A new peak was generated after reducing at 300 nm that attributed to the formation of 4-aminophenol and regularly enhanced to lighten the yellow color of the reaction solution.

Furthermore, for the reusability of the synthesized catalyst, the external magnet was used and separated the magnetic catalyst completely from the reaction mixture without any variation in catalytic activity. The advantages of this method for the reduction of the organic pollutant and employing the organometallic biocatalyst $Ag/Fe_3O_4/CdO$@MWCNTs are the effectiveness, ecological type, and inexpensive process for the removal and photo decreasing of 4-NP.

Evaluation of the antioxidant property of prepared spiropyridoindolpyrrolidines by DPPH

Another purpose of this research is the study of the antioxidant property of synthesized spiropyridoindolpyrrolidines, and for achieving to this goal, DPPH was used. It should be mentioned that the DPPH radical scavenging test was employed for many purposes such as for studying the antioxidant activity of synthesized organic compounds, foods, and biological structures (Ahmadi et al., 2007; Bidchol et al., 2011; Saundane and Nandibeoor, 2015) *via* taking an electron or hydrogen atom by the free radical of DPPH. The synthesized spiropyridoindolepyrrolidine loses the hydrogen atom or one electron in the presence of the DPPH radical, and this means that these compounds have antioxidant property. The percentage of trapping the DPPH free radical by the synthesized spiropyridoindolpyrrolidines displays the order of antioxidant activity. In this research, we investigated the antioxidant activity of some synthesized compounds such as **7a-7d** and compared to standard synthesized antioxidant BHT and TBHQ, in which the electron or hydrogen absorbance of these compounds by DPPH free radical proved the antioxidant activity of them. When one electron or hydrogen atom is adsorbed by DPPH, the absorbance of it decreases to 517 nm. Overall, the antioxidant ability of spiropyridoindolepyrrolidine derivatives **7a-7d** was achieved as TBHQ¯BHT>**7b** > **7d**> **7c** > **7a** (Figure 6).

Figure 8 exhibited that good differences existed between spiropyridoindolepyrrolidines concentration to BHT and TBHQ as the standard antioxidant. Compound **7b** showed good ability relative o BHT and TBHQ among the experimented spiropyridoindolepyrrolidines **7a-7d**,

Assessment of spiropyridoindolepyrrolidines' antioxidant activity by Fe^{3+} reduction

The antioxidant property of spiropyridoindolepyrrolidines **7a-7d** was tested by another procedure for confirming it. The spiropyridoindolepyrrolidines caused the reduction of ferric ions (Fe^{3+}), and the amounts of reduction are measured based on the reduction of Fe^{3+}/ferricyanide to the Fe^{2+}/ferrous at 700 nm (Yildirim et al., 2001), and spiropyridoindolpyrrolidines **7b** exhibited good effect than BHT and TBHQ. Figure 7 shows the order of the antioxidant activity of spiropyridoindolepyrrolidines **7a-7d** as TBHQ > BHT>**7b** > **7a**>**7c** > **7d**.

Antibacterial activity evaluation of synthesized spiropyridoindolepyrrolidines

For the investigation of the antibacterial activity of synthesized compounds, two antibiotic drugs such as streptomycin and gentamicin were employed, and the results of the antimicrobial activity of synthesized compounds compared with two standards are displayed in Table 4 and Figure 8. For the evaluation of this experiment, two suitable and significant factors that effect the diameter and inhibition zone are the type of bacteria and concentration of synthesized spiropyridoindolepyrrolidines.

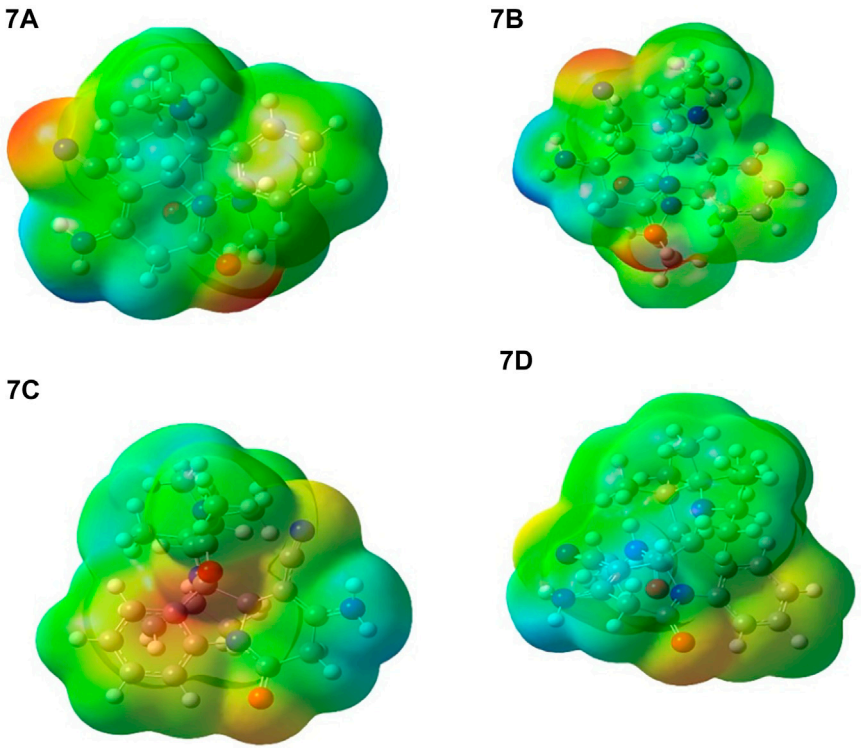

FIGURE 12
Calculated molecular electrostatic potential surfaces for **7a-7d**.

Spiropyridoindolepyrrolidines **7a-7g** have good diameter and inhibition zone owing to the effect of *Escherichia coli*, among the Gram-positive and -negative bacteria (Figure 8).

3 Molecular geometry

An optimized structure with a numbering scheme is shown in Figure 9. For the four compounds studied, the bond lengths of C-H bonds are calculated as 1.08–1.10 Å. The C-N bond length for the four states in the range of 1.36–1.45 Å C25-N26 bond length is considerably shorter than other C-N bond lengths because of the hybridization of sp. The C16 = O17, C23 = O24 bond lengths are calculated as 1.22–1.23 Å. The sp^3 hybridized carbon atom bonded with C22 (sp^2)—C21 (sp^3) atoms shows their bond lengths 1.49 Å and 1.50 Å, respectively. The bond length of C20 (sp^2)—C21 (sp^2) is 1.36 Å, which is slightly lower and shows its double bond character.

Mulliken atomic charges

The atomic charges were calculated by Mulliken atomic charges (Mulliken, 1955). The electronic charge on atoms within a molecule is a crucial factor to decide the bonding capability of the molecule. The net atomic charge in the molecule provides a picture of electron density distribution over the molecule. The distribution of Mulliken atomic charge is listed in Table 5 and shown in Figure 10. The Mulliken atomic charges on carbon atoms reveal either the positive or negative value. All hydrogen atoms showed a net positive charge, but H_{46}, H_{47}, and H_{51} obtained high value positive charge than the other hydrogen atoms, due to the presence of an electronegative atom (N). All oxygen atoms of the optimized compound were shown to have a negative charge, which act as donor atoms. The results are reported in Table 5 of atoms attached to a high electronegative atom.

HOMO–LUMO analysis and global reactivity descriptors

HOMO and LUMO are important parameters used in quantum chemistry. The difference between the energies of HOMO and LUMO is referred as the energy gap, which determines the reactivity and kinetic stability of molecules (Venkatesh et al., 2016). The HOMO–LUMO energy gap value for title compounds is given in Table 6. The pictorial

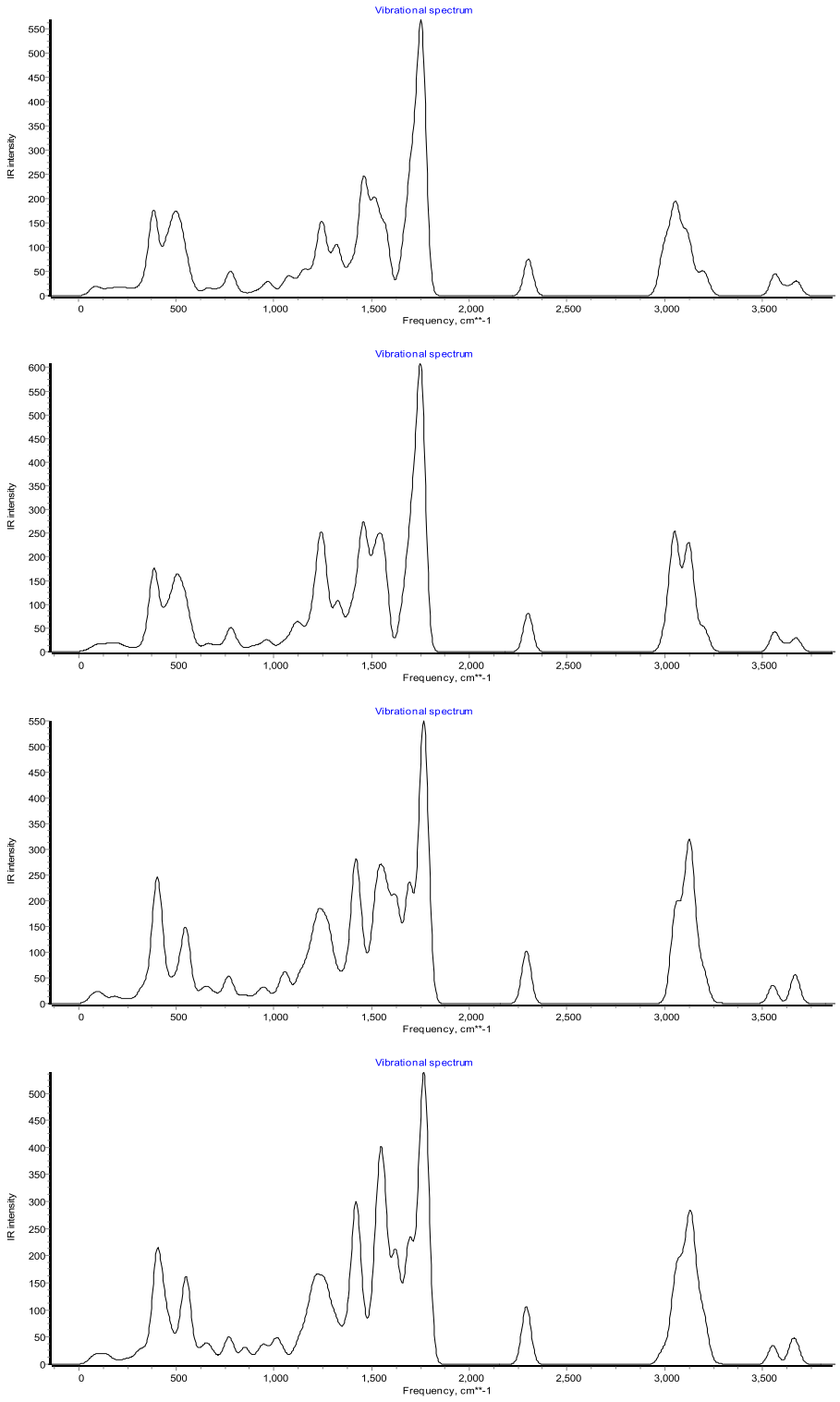

FIGURE 13
Plot vibration spectrum for **7a-7d** compounds.

illustration of the frontier molecular orbitals with their energies is shown in Figure 11. Furthermore, HOMO orbitals are mostly localized on Spiro and phenyl rings, while LUMO orbitals were located partially on carbonyl, but mostly located near the phenyl ring.

Density functional theory-based global chemical reactivity descriptors such as the chemical potential (μ), chemical hardness (η), global softness (S), and electrophilicity index (ω) have been calculated for four compounds, given in Table 7. The values of chemical potential (μ) indicated that 7b compound is higher than 7a, 7c, and 7d compounds; it means that 6d compounds increase reactivity. The hardness of 7a and 7c compounds decreased, but for 7b and 7d, the chemical hardness increased. The electrophilicity by 7c and 7d compounds increases, but for 7a and 7b compounds, the electrophilicity decreased. Global chemical reactivity descriptors are used to understand the relationship between structure, stability, and global chemical reactivity of compounds. The small values of η are said to be chemically soft (S) and are highly polarizable and more chemically reactive. The chemical potential (μ) measures the escaping tendency of electrons from a compound in its ground state. High values of chemical potential signify that the molecule is less stable and more reactive (Mebi, 2011). The global electrophilicity index (ω) measures the stabilization in energy of a system, when it acquires an additional electronic charge from the environment. The results of the four compounds studied revealed that 6b has high reactivity, and the resultant antioxidant ability showed good activity that **7b > 7c > 7a>7d.**

Molecular electrostatic potential surface

The molecular electrostatic potential (MEP) is used to predict the relative reactivity positions in a species for nucleophilic and electrophilic attack. The electrostatic potential surface map of the studied compound is given in Figure 12. The color of the compounds is in the range of $-0.144e^{-2}$ to $+0.144e^{-2}$. The red and blue color in the MEP structure point to more electron-rich and electron-poor region, respectively. In the MEP, the negative potential regions are localized over the electronegative atoms (oxygen and nitrogen) and the positive potential regions are localized over the carbon and hydrogen atoms and phenyl ring. However, the nitrogen atom of the compound is a less-negative potential site than the other electronegative atoms. Therefore, the more-negative potential and positive electrostatic potential sites are more favorable for the attraction of nucleophilic and electrophilic species.

Vibrational assignments

There are a total of 53–68 atoms in **7a-7d** compounds with 153–198 fundamental modes of vibration. The experimental FTIR spectrum was obtained from this article. Theoretically, frequencies are predicted by the DFT/B3LYP method using the 6–311++G** basis set. The theoretically predicted vibrational frequencies are scaled by an empirical factor 0.9613 (Foresman and Frisch, 1996). The infrared stretching frequencies of these groups vary in the same order, ranging from 1,222–1,254 cm^{-1} for C-N and 2,210 cm^{-1} for C=N (cyanide). The experimental C=O stretching frequency appeared at 1767–1779 cm^{-1}, and theoretically, it is observed at 1,684–1,687 cm^{-1}. Computed frequencies at 3,000–3,264 cm^{-1} indicate C-H stretching. The aromatic C=C stretching frequency theoretically appeared at 1,664 cm^{-1} and 1,651–1,656 for C=C aromatic, which is close to the experimental values. Also, frequencies at 3,421 and 3,528 cm^{-1} for NH stretching in Figure 13 show all vibration spectra.

4 Conclusion

In summary, we have investigated an effective, green, and environment-friendly reaction including isatins, activated acetylenic compounds, alkyl bromides, ammonium acetate, isothiocyanates, and aziridine in aqueous media at ambient temperature in the presence of a new organometallic nanocatalyst $Ag/Fe_3O_4/CdO$@MWCNT-MNC, which has produced new derivatives of spiropyridoindolepyrrolidines. Also, two methods were employed for the evaluation of the antioxidant power of the synthesized spiropyridoindolepyrrolidines **7a-7d** which confirmed that the synthesized compounds have good antioxidant ability relative to standard antioxidants. In addition, for the investigation of the antibacterial activity of synthesized compounds, Gram-positive and -negative bacteria were utilized, and the disk diffusion process was used for the confirmation of the antimicrobial ability of the produced spiropyridoindolepyrrolidines. The results of antimicrobial activity investigation displays that synthesized spiropyridoindolepyrrolidines have good biological activity and could avoid the bacterial growth. As a result, this procedure that is used for the synthesis of spiropyridoindolepyrrolidines have some advantages such as reaction with high rate, high yield product, green process, employing little amounts of catalyst, easy separation of organometallic catalyst from the reaction mixture, and easy product purification that are the important points in these reactions.

5 Experimental

General

In this research work, all the starting materials that are needed for the synthesis of spiropyridoindolepyrrolidines and

also reagents and solvents were prepared from Fluka and Merck Company without any purification. For the synthesis of the nanocatalyst, MWCNTs that have 8 nm diameter are used, of 30 μm for length and 95% for purity, and prepared from Merck Company. For approving the construction of synthesized catalyst Ag/Fe_3O_4/CdO@MWCNT MNCs, the spectroscopy analysis such as XRD, SEM, EDX, and VSM was utilized. The FT-IR (KBr medium) of synthesized spiropyridoindolepyrrolidines was taken by using the Shimadzu IR-460 spectrometer instrument. Additionally, another way for the confirmation of the structure of synthesized compounds giving ^{1}H-NMR and ^{13}C-NMR with the Bruker DRX-500 AVANCE spectrometer instrument with 500 MHz NMR in $CDCl_3$ as solvent and TMS as internal standard was used. Mass spectra for synthesized compounds were given by the Finnigan, MAT 8430 spectrometer with an ionization potential 70 eV. For the determination of elements in the prepared compounds, the Heraeus CHN–O-Rapid analyzer was employed.

Generation of *Petasites hybridus* rhizome water extract

Petasites hybridus rhizome was dried, and 10 g of it was poured in a two-neck round-bottom flask (250 ml), and water (100 ml) was added, and the new mixture was stirred at 100°C and filtered after 2 h. For the production of the nanocomposite, the water extract of *Petasites hybridus* rhizome and other compounds was employed as follows.

Generation of Ag/Fe_3O_4/CdO@MWCNT MNCs (Rajendran and Sengodan, 2017)

The mixture of Cd $(NO_3)_2$ (1.5 g) and $FeCl_2.4H_2O$ (1.5 g) were dissolved in water (10 ml), and then, the *Petasites hybridus* rhizome water extract (5 ml) was added easily to the previous mixture, and the temperature of the mixture was enhanced to 100°C in a round-bottom flask and mixed for 5 h When the reaction was completed, the temperature of the reaction was reduced to room temperature. Then, after cooling, for deleting the undesired organic compounds, the reaction mixture was sonicated for 30 min and centrifuged at 7,000 rpm for about 10 min. After this, $AgNO_3$ (1.5 g) was poured in the previous mixture, and sonication of the new mixture was continued at 100°C for 45 min, and Ag/Fe_3O_4/CdO MNCs was synthesized. For the synthesis of Ag/Fe_3O_4/CdOQMWCNTs MNCs, the MWCNTs (0.1 g) and Ag/Fe_3O_4//CdO MNCs (0.1 g) prepared in the previous section were added to 100 ml water extract of *Petasites hybridus* rhizome and mixed at 150°C for 1 h. Centrifugation was used for the separation of colloid and then washed with water, dried, and calcinated at 300°C for 45 min. After this, the Ag/Fe_3O_4/CdO @MWCNT magnetic nanocomposite was produced, which was cooled to room temperature and washed with a mixture of water and ethanol (50:50) several times. After washing the solid, by employing an external magnet, the catalyst was separated and dried at room temperature for 24 h.

Preparation process of spiropyridoindolepyrrolidine 7a–l

Isatines **1** (2 mmol), acetyl chloride **2** (2 mmol), and Ag/Fe_3O_4/CdO@MWCNT (0.02 g) were added to water as solvent at room temperature and mixed for 30 min. Secondary amines **3** (2 mmol) were poured to the previous mixture after 30 min, and the new mixture was mixed for 20 min. Vinilidene Meldrum's acid **4** (2 mmol) and amines **5** (2 mmol) were added to the previous mixture and stirred for 30 min. Finally, malonnnitrile **6** (2 mmol) was added, and the final mixture was stirred for 45 min in the presence of a catalyst. Completion of the reaction took place after 3 h and monitored by TLC; in this stage, separation was performed with an external magnet, and solid residue was washed by EtOH and Et_2O to prepare purified spiropyridoindolepyrrolidine **7** (see Supplementary Material).

8-Amino-9-cyano-N,1′,4′,4′-tetramethyl-6-oxo-6H-spiro[pyrido[1,2-a]indole-10,2′-pyrrolidine]-3′-carboxamide **(7a):** yellow powder, m. p. 135–137°C, 0.72 g, yield 95%. IR (KBr) (ν_{max}/cm^{-1}): 3,456, 1,732, 2,198, 1,698, 1,624, 1,456, and 1,230 cm^{-1}.^{1}H NMR (500 MHz, $CDCl_3$): δ 1.05 (3 H, s, Me), 1.10 (3 H, s, Me), 2.39 (3 H, s, NMe), 2.76 (3 H, s, NMe), 2.82 (1 H, d, $^2J_{HH}$ = 8.0 Hz, CH), 3.04 (1 H, d, $^2J_{HH}$ = 8.0 Hz, CH), 3.64 (1 H, s, CH), 5.68 (1 H, s, CH), 7.08 (1 H, t, $^3J_{HH}$ = 7.6 Hz, CH), 7.20 (1 H, d, $^3J_{HH}$ = 8.0 Hz, CH), 7.39 (1 H, t, ^3J = 7.6 Hz, CH), 7.51 (1 H, d, ^3J = 7.6 Hz, CH), 9.87 (1 H, s, NH), and 10.23 (2 H, s, NH_2) ppm. ^{13}C NMR (125.7 MHz, $CDCl_3$): δ 25.56, 25.95, 38.06, 40.29, 63.08, 65.10, 70.20, 79.57, 95.19, 115.18, 117.01, 123.20, 124.24, 128.55, 133.86, 136.93, 154.40, 160.91, 160.92, and 171.97 ppm. MS, *m/z* (%): 377 (M^+, 10), 319 (48), and 58 (100). Anal. Calcd for $C_{21}H_{23}N_5O_2$ (377.45): C, 66.83; H, 6.14; N, 18.55; Found: C, 66.92; H, 6.23; N, 18.74%.

8-Amino-9-cyano-N,1′-diethyl-4′,4′,5′-trimethyl-6-oxo-6H-spiro[pyrido[1,2-a]indole-10,2′-pyrrolidine]-3′-carboxamide **(7b):** yellow powder, m. p. 142–144°C, 0.76 g, yield 90%. IR (KBr) (ν_{max}/cm^{-1}): 3,457, 1,732, 2,196, 1,697, 1,626, 1,585, and 1,227 cm^{-1}.^{1}H NMR (500 MHz, $CDCl_3$): δ 1.02 (3 H, s, Me), 1.07 (3 H, s, Me), 1.10 (3 H, d, $^3J_{HH}$ = 8.0 Hz, Me), 1.19 (3 H, t, $^3J_{HH}$ = 7.4 Hz, Me),1.22 (3 H, t, $^3J_{HH}$ = 7.4 Hz, Me), 2.81–2.86 (1 H, m, CH), 2.96–3.01 (1 H, m, CH), 3.20–3.27 (3 H, m, 3 CH), 3.67 (1 H, s, CH), 5.68 (1 H, s, CH), 7.08 (1 H, t, $^3J_{HH}$ = 7.6 Hz, CH), 7.19 (1 H, d, $^3J_{HH}$ = 7.6 Hz, CH), 7.39 (1 H, t, ^3J = 7.6 Hz, CH), 7.52 (1 H, d, ^3J = 7.6 Hz, CH), 10.04 (1 H, s, NH), and 10.37 (2 H, s, NH_2) ppm. ^{13}C NMR (125.7 MHz, $CDCl_3$): δ 14.61, 14.70, 15.44, 23.76, 35.51, 41.32, 42.38, 61.91, 65.14, 70.19, 77.47, 95.19, 115.18, 117.01, 123.17, 124.19, 128.65, 133.90, 136.72, 154.51, 160.91, 161.83, and 171.24 ppm. MS,

m/z (%): 419 (M^+, 15), 347 (38), and 72 (100). Anal. Calcd for $C_{24}H_{29}N_5O_2$ (419.53): C, 68.71; H, 6.97; N, 16.69; Found: C, 68.83; H, 7.06; N, 16.83%.

***8-Amino-9-cyano-1′-isopropyl-N,4′,4′,5′,5′-pentamethyl-6-oxo-6H-spiro[pyrido[1,2-a]indole-10,2′-pyrrolidine]-3′-carboxamide* (7c):** yellow powder, m. p. 152–154°C, 0.78 g, yield 90%. IR (KBr) (ν_{max}/cm^{-1}): 3,458, 2,217, 1719, 1,694, 1,628, 1,597 and 1,257 cm^{-1}.^{1}H NMR (500 MHz, $CDCl_3$): δ 1.08 (3 H, s, Me), 1.13 (3 H, s, Me), 1.16 (6 H, d, $^3J_{HH}$ = 7.2 Hz, 2 Me), 1.22 (3 H, s, Me), 1.27 (3 H, s, Me), 2.76 (3 H, s, NMe), 3.57–3.61 (1 H, m, CH), 3.71 (1 H, s, CH), 5.67 (1 H, s, CH), 7.06 (1 H, t, $^3J_{HH}$ = 7.6 Hz, CH), 7.21 (1 H, d, $^3J_{HH}$ = 7.6 Hz, CH), 7.42 (1 H, t, ^3J = 7.6 Hz, CH), 7.52 (1 H, d, ^3J = 7.6 Hz, CH), 10.07 (1 H, s, NH), 10.42 (2 H, s, NH_2) ppm.^{13}C NMR (125.7 MHz, $CDCl_3$): δ 22.51, 23.39, 23.99, 25.95, 46.83, 47.38, 55.30, 67.80, 70.12, 78.33, 95.19, 115.19, 117.01, 123.34, 124.15, 128.74, 134.33, 136.96, 154.51, 160.91, 161.65, 172.50 ppm. MS, *m/z* (%): 433 (M^+, 15), 375 (48), 58 (100). Anal. Calcd for $C_{25}H_{31}N_5O_2$ (433.56): C, 69.26; H, 7.21; N, 16.15; Found: C, 69.38; H, 7.32; N, 16.26%.

***8-Amino-9-cyano-N-ethyl-1′-isopropyl-4′,4′,5′,5′-tetramethyl-6-oxo-6H-spiro [pyrido[1,2-a]indole-10,2′-pyrrolidine]-3′-carboxamide* (7d):** yellow powder, m. p. 163–165°C, 0.78 g, yield 87%. IR (KBr) (ν_{max}/cm^{-1}): 3,464, 2,184, 1,719, 1,694, 1,628, 1,597, and 1,257 cm^{-1}.^{1}H NMR (500 MHz, $CDCl_3$): δ 1.08 (3 H, s, Me), 1.13 (3 H, s, Me), 1.17 (6 H, d, $^3J_{HH}$ = 6.8 Hz, 2 Me), 1.22 (3 H, s, Me), 1.23 (3 H, t, $^3J_{HH}$ = 7.4 Hz, Me), 1.27 (3 H, s, Me), 3.21–3.27 (2 H, m, CH_2N), 3.58–3.61 (1 H, m, CH), 3.75 (1 H, s, CH), 5.68 (1 H, s, CH), 7.08 (1 H, t, $^3J_{HH}$ = 7.7 Hz, CH), 7.22 (1 H, d, $^3J_{HH}$ = 7.7 Hz, CH), 7.42 (1 H, t, ^3J = 7.7 Hz, CH), 7.53 (1 H, d, ^3J = 7.6 Hz, CH), 9.87 (1 H, s, NH), and 10.23 (2 H, s, NH_2) ppm. ^{13}C NMR (125.7 MHz, $CDCl_3$): δ 14.70, 22.51, 23.39, 23.99, 35.51, 46.67, 47.38, 54.94, 67.80, 70.12, 78.46, 95.19, 115.19, 117.01, 123.34, 124.15, 128.74, 134.33, 136.96, 154.51, 160.91, 161.65, and 172.04 ppm. MS, *m/z* (%): 447 (M^+, 15), 375 (48), and 72 (100). Anal. Calcd for $C_{26}H_{33}N_5O_2$ (447.58): C, 69.77; H, 7.43; N, 15.65; Found: C, 69.83; H, 7.52; N, 15.73%.

***8-Amino-9-cyano-N-ethyl-1′,4′-dimethyl-6-oxo-6H-spiro [pyrido[1,2-a]indole-10,2′-pyrrolidine]-3′-carboxamide* (7e):** yellow powder, m. p. 151–153°C, 0.66 g, yield 87%. IR (KBr) (ν_{max}/cm^{-1}): 3,468, 2,196, 1,716, 1,696, 1,663, 1,547, 1,473, and 1,228 cm^{-1}.^{1}H NMR (500 MHz, $CDCl_3$): δ 1.07 (3 H, d, $^3J_{HH}$ = 8.0 Hz, Me), 1.23 (3 H, t, $^3J_{HH}$ = 7.4 Hz, Me), 2.30–2.35 (1 H, m, CH), 2.44 (NCH_3), 3.02 (2 H, m, CH_2), 3.22 (2 H, q, $^3J_{HH}$ = 7.4 Hz, CH_2N), 3.55–3.57 (1 H, m, CH), 5.65 (1 H, s, CH), 7.06 (1 H, t, $^3J_{HH}$ = 7.7 Hz, CH), 7.22 (1 H, d, $^3J_{HH}$ = 7.6 Hz, CH), 7.40 (1 H, t, ^3J = 7.6 Hz, CH), 7.52 (1 H, d, ^3J = 7.6 Hz, CH), 10.12 (1 H, s, NH), and 10.56 (2 H, s, NH_2) ppm. ^{13}C NMR (125.7 MHz, $CDCl_3$): δ 14.70, 16.52, 32.15, 35.61, 39.39, 54.34, 59.46, 70.32, 79.07, 95.22, 115.17, 117.01, 123.41, 124.18, 128.54, 133.12, 137.28, 154.40, 160.91, 161.54, and 174.46 ppm. MS, *m/z* (%): 377 (M^+, 10), 375 (68), and 72 (100). Anal. Calcd for $C_{21}H_{23}N_5O_2$ (377.45): C, 66.83; H, 6.14; N, 18.55; Found: C, 66.92; H, 6.34; N, 18.68%.

***8-Amino-9-cyano-N,1′,4′-trimethyl-6-oxo-6H-spiro [pyrido[1,2-a]indole-10,2′-pyrrolidine]-3′-carboxamide* (7f):** yellow powder, m. p. 147–149°C, 0.64 g, yield 87%. IR (KBr) (ν_{max}/cm^{-1}): 3,457, 2,213, 1,716, 1,697, 1,663, 1,547, 1,473, and 1,228 cm^{-1}.^{1}H NMR (500 MHz, $CDCl_3$): δ 1.07 (3 H, d, $^3J_{HH}$ = 8.0 Hz, Me), 2.31–2.36 (1 H, m, CH), 2.45 (NCH_3), 2.76 (NCH_3), 3.02 (2 H, m, CH_2), 3.58–3.60 (1 H, m, CH), 5.68 (1 H, s, CH), 7.06 (1 H, t, $^3J_{HH}$ = 7.7 Hz, CH), 7.23 (1 H, t, $^3J_{HH}$ = 7.6 Hz, CH), 7.38 (1 H, d, ^3J = 7.6 Hz, CH), 7.52 (1 H, d, ^3J = 7.6 Hz, CH), 10.15 (1 H, s, NH), and 10.63 (2 H, s, NH_2) ppm.^{13}C NMR (125.7 MHz, $CDCl_3$): δ 16.52, 25.98, 32.10, 39.39, 53.73, 59.46, 70.32, 79.07, 95.22, 115.17, 117.01, 123.41, 124.18, 128.54, 133.12, 137.28, 154.40, 160.91, 161.54, and 174.96 ppm. MS, *m/z* (%): 363 (M^+, 10), 375 (68), and 45 (100). Anal. Calcd for $C_{20}H_{21}N_5O_2$ (363.42): C, 66.10; H, 5.82; N, 19.27; Found: C, 66.25; H, 5.93; N, 19.34%.

***8-Amino-9-cyano-N,1′-dimethyl-6-oxo-4′-phenyl-6H-spiro [pyrido[1,2-a]indole-10,2′-pyrrolidine]-3′-carboxamide* (7g):** yellow powder, m. p. 171–173°C, 0.77 g, yield 90%. IR (KBr) (ν_{max}/cm^{-1}): 3,387, 2,198, 1,710, 1,695, 1,635, 1,460, 1,213, and 1,092 cm^{-1}.^{1}H NMR (500 MHz, $CDCl_3$): δ 2.44 (3 H, s, NMe), 2.75 (3 H, s, NMe), 3.15–3.18 (1 H, m, CH), 3.41–3.45 (1 H, m, CH), 3.51–3.53 (1 H, m, CH), 3.69 (1 H, d, ^3J = 6.7 Hz, CH), 5.68 (1 H, s, CH), 7.07 (1 H, t, $^3J_{HH}$ = 7.8 Hz, CH), 7.22–7.29 (6 H, m, 6 CH), 7.40 (1 H, t, ^3J = 7.8 Hz, CH), 7.52 (1 H, d, ^3J = 7.8 Hz, CH), 10.15 (1 H, s, NH), and 10.38 (2 H, s, NH_2) ppm. ^{13}C NMR (125.7 MHz, $CDCl_3$): δ 25.96, 39.43, 44.49, 55.58, 56.88, 70.32, 78.05, 95.19, 115.17, 117.01, 123.43, 124.14, 126.20, 126.81, 128.54, 128.60, 132.73, 137.13, 139.91, 154.50, 160.91, 161.46, and 174.52 ppm. MS, *m/z* (%): 425 (M^+, 10), 77 (54), and 58 (100). Anal. Calcd for $C_{25}H_{23}N_5O_2$ (425.49): C, 70.57; H, 5.45; N, 16.46; Found: C, 70.68; H, 5.56; N, 16.57%.

***8-Amino-9-cyano-N-(4-methoxybenzyl)-1′,4′-dimethyl-6-oxo-6H-spiro[pyrido[1,2-a]indole-10,2′-pyrrolidine]-3′-carboxamide* (7h):** yellow powder, m. p. 167–169°C, 0.80 g, yield 85%. IR (KBr) (ν_{max}/cm^{-1}): 3,689, 2,132, 1,716, 1,697.3, 1,663, 1,547, 1,473, and 1,228 cm^{-1}.^{1}H NMR (500 MHz, $CDCl_3$): δ 1.07 (3 H, d, $^3J_{HH}$ = 8.0 Hz, Me), 2.30–2.35 (1 H, m, CH), 2.44 (3 H, s, NMe), 3.02 (2 H, m, CH_2), 3.60–3.62 (1 H, m, CH), 3.78 (3 H, s, MeO), 4.42 (2 H, s, CH_2), 5.69 (1 H, s, CH), 6.85 (2 H, d, ^3J = 7.8 Hz, 2 CH), 7.06 (1 H, t, ^3J = 7.6 Hz, CH), 7.18 (2 H, d, $^3J_{HH}$ = 7.8 Hz, 2 CH), 7.23 (1 H, d, $^3J_{HH}$ = 7.6 Hz, CH), 7.38 (1 H, t, ^3J = 7.6 Hz, CH), 7.52 (1 H, d, ^3J = 7.6 Hz, CH), 9.86 (1 H, s, NH), and 10.37 (2 H, s, NH_2) ppm. ^{13}C NMR (125.7 MHz, $CDCl_3$): δ 16.52, 32.15, 39.39, 44.15, 54.61, 55.33, 59.46, 70.32, 79.10, 95.22, 113.79, 115.17, 117.01, 123.41, 124.18, 128.54, 128.78, 133.13, 133.98, 137.28, 158.76, 154.40, 160.91, 161.54, and 173.66 ppm. MS, *m/z* (%): 495 (M^+, 10), 375 (54), and 121 (100). Anal. Calcd for $C_{27}H_{27}N_5O_3$ (469.55): C, 69.07; H, 5.80; N, 14.92; Found: C, 68.82; H, 6.14; N, 11.97%.

8-Amino-9-cyano-N,4′,4′,5′-tetramethyl-1′-(4-nitrophenyl)-6-oxo-6H-spiro[pyrido [1,2-a]indole-10,2′-pyrrolidine]-3′-carboxamide **(7i):** orange powder, m. p. 183–185°C, 0.72 g, yield 75%. IR (KBr) (ν_{max}/cm^{-1}): 3,468, 2,198, 1,710, 1,698, 1,628, 1,439, and 1,219 cm^{-1}.^{1}H NMR (500 MHz, $CDCl_3$): δ 1.03 (3 H, s, Me), 1.08 (3 H, s, Me), 1.22 (3 H, d, ^3J = 6.8 Hz, Me), 2.75 (3 H, s, NMe), 3.74 (1 H, s, CH), 4.06 (1 H, q, ^3J = 6.8 Hz, CH), 5.71 (1 H, s, CH), 6.98 (2 H, d, ^3J = 7.8 Hz, 2 CH), 7.10 (1 H, t, ^3J = 7.6 Hz, CH), 7.23 (1 H, d, $^3J_{HH}$ = 7.6 Hz, CH), 7.42 (1 H, t, $^3J_{HH}$ = 7.6 Hz, CH), 7.52 (1 H, d, ^3J = 7.6 Hz, CH), 8.08 (2 H, d, ^3J = 7.6 Hz, 2 CH), 10.03 (1 H, s, NH), and 10.28 (2 H, s, NH_2) ppm. ^{13}C NMR (125.7 MHz, $CDCl_3$): δ 14.88, 24.10, 25.95, 44.98, 63.34, 64.74, 69.91, 78.36, 95.58, 115.19, 116.27, 117.02, 124.21, 124.59, 125.34, 128.77, 133.16, 136.70, 144.43, 151.03, 154.13, 161.44, 163.21, and 171.36 ppm. MS, *m/z* (%): 498 (M$^+$, 15), 440 (52), and 58 (100). Anal. Calcd for $C_{27}H_{26}N_6O_4$ (498.5452): C, 65.05; H, 5.26; N, 16.86; Found: C, 65.18; H, 5.38; N, 16.97%.

8-Amino-9-cyano-N,4′,4′-trimethyl-6-oxo-1′-(p-tolyl)-6H-spiro[pyrido[1,2-a]indole-10,2′-pyrrolidine]-3′-carboxamide **(7j):** pale orange powder, m. p. 177–179°C, 0.73 g, yield 80%. IR (KBr) (ν_{max}/cm^{-1}): 3,437, 2,214, 1,744, 1,697, 1,634, 1,573, 1,439, and 1,215 cm^{-1}.^{1}H NMR (500 MHz, $CDCl_3$): δ 1.08 (3 H, d, ^3J = 6.8 Hz, Me), 2.28 (3 H, s, Me), 2.31–2.34 (1 H, m, CH), 2.35 (3 H, s, Me), 2.75 (3 H, s, NMe), 3.66–3.79 (3 H, m, 3 CH), 5.71 (1 H, s, CH), 6.84 (2 H, d, $^3J_{HH}$ = 7.8 Hz, 2 CH), 7.03 (2 H, d, $^3J_{HH}$ = 7.8 Hz, 2 CH), 7.09 (1 H, s, CH), 7.19 (1 H, d, $^3J_{HH}$ = 7.6 Hz, CH), 7.36 (1 H, d, ^3J = 7.6 Hz, CH), 9.85 (1 H, s, NH), and 10.67 (2 H, s, NH_2) ppm. ^{13}C NMR (125.7 MHz, $CDCl_3$): δ 20.71, 25.50, 25.95, 43.13, 58.77, 65.98, 69.89, 79.02, 95.58, 115.18, 116.26, 117.02, 124.10, 124.22, 128.76, 129.33, 130.82, 133.18, 136.94, 144.69, 154.13, 161.44, 161.87, and 171.79 ppm. MS, *m/z* (%): 453 (M$^+$, 10), 395 (68), and 58 (100). Anal. Calcd for $C_{27}H_{27}N_5O_2$ (453.55): C, 71.50; H, 6.00; N, 15.44; Found: C, 71.63; H, 6.18; N, 15.52%.

8-Amino-9-cyano-4′-ethyl-N,1′,2,4′-tetramethyl-6-oxo-6H-spiro[pyrido[1,2-a]indole-10,2′-pyrrolidine]-3′-carboxamide **(7k):** yellow powder, m. p. 1201–203°C, yield 75%. IR (KBr) (ν_{max}/cm^{-1}): 3,547, 3,387, 1735, 1,698, 1,678, 1,576, 1,487 and 1,295 cm^{-1}.^{1}H NMR (500 MHz, $CDCl_3$): δ 0.82 (3 H, t, $^3J_{HH}$ = 7.4 Hz, Me), 1.05 (3 H, s, Me), 1.47–1.49 (1 H, m, CH), 1.58–1.63 (1 H, m, CH), 2.28 (3 H, s, Me), 2.37 (3 H, s, NMe), 2.76 (3 H, s, NMe), 2.78 (1 H, d, ^2J = 6.3 Hz, CH), 3.00 (1 H, d, ^2J = 6.3 Hz, CH), 3.66 (1 H, s, CH), 5.68 (1 H, s, CH), 7.07 (1 H, s, CH), 7.18 (1 H, d, $^3J_{HH}$ = 7.8 Hz, CH), 7.31 (1 H, d, $^3J_{HH}$ = 7.8 Hz, CH), 10.23 (1 H, s, NH), 10.64 (2 H, s, NH_2) ppm. ^{13}C NMR (125.7 MHz, $CDCl_3$): δ 8.55, 21.28, 22.21, 25.95, 30.82, 38.05, 41.04, 54.32, 62.76, 70.20, 77.80, 95.19, 114.19, 117.01, 123.59, 128.84, 134.48, 135.24, 135.64, 154.50, 160.91, 160.93, 172.05 ppm. MS, *m/z* (%): 405 (M$^+$, 10), 395 (68), 58 (100). Anal. Calcd for $C_{23}H_{27}N_5O_2$ (405.50): C, 68.13; H, 6.71; N, 17.27; Found: C, 68.32; H, 6.34; N, 17.42%.

8-Amino-9-cyano-1′,2,4′,4′-tetramethyl-6-oxo-N-phenyl-6H-spiro[pyrido[1,2-a]indole-10,2′-pyrrolidine]-3′-carboxamide **(7l):** yellow powder, m. p. 196–198°C, yield 85%. IR (KBr) (ν_{max}/cm^{-1}): 3,567, 3,468, 1,738, 1,695, 1,639, 1,578, 1,468, and 1,298 cm^{-1}.^{1}H NMR (500 MHz, $CDCl_3$): δ 1.05 (3 H, s, Me), 1.10 (3 H, s, Me), 2.28 (3 H, s, Me), 2.39 (3 H, s, NMe), 2.82 (1 H, d, ^3J = 8.0 Hz, CH), 3.04 (1 H, d, ^3J = 8.0 Hz, CH), 3.67 (1 H, s, CH), 5.68 (1 H, s, CH), 7.06–7.19 (3 H, m, 3 CH), 7.31–7.37 (3 H, m, 3 CH), 7.49 (2 H, d, $^3J_{HH}$ = 7.6 Hz, 2 CH), 10.17 (1 H, s, NH), and 10.54 (2 H, s, NH_2) ppm. ^{13}C NMR (125.7 MHz, $CDCl_3$): δ 21.28, 25.57, 38.06, 40.99, 63.04, 66.79, 70.20, 79.37, 95.19, 114.19, 115.56, 120.92, 123.59, 124.48, 128.84, 129.03, 134.48, 134.65, 135.56, 138.48, 154.50, 160.91, 160.96, and 171.63 ppm. MS, *m/z* (%): 453 (M$^+$, 10), 395 (68), and 58 (100). Anal. Calcd for $C_{27}H_{27}N_5O_2$ (453.55): C, 71.50; H, 6.00; N, 15.44; Found: C, 71.62; H, 6.18; N, 15.63; %.

Common process for the generation of spiropyrrolopyridine 17a–d

Spiropyridoindolepyrrolidine **7** (2 mmol) prepared in previous reactions was mixed in water with ethylbromopyruvate **15** (2 mmol) and Ag/Fe_3O_4/CdO@MWCNT (0.02 g) for 45 min at room temperature. After this, the dimethyl acetylenedicarboxylate **16** (2 mmol) was added to the previous mixture, and the new mixture was stirred for 3 h. The completion of reaction was monitored by TLC, and the solid residue was separated by filtration and cleaned with EtOH and Et_2O to afford purified spiropyridine **17**.

4-Ethyl 2,3-dimethyl 1′,4′,4′-trimethyl-3′-(methylcarbamoyl)-7-oxo-5,7-dihydrospiro[pyrido [2′′,3′′:4′,5′]pyrrolo[3′,2′:3,4]pyrido[1,2-a]indole-13,2′-pyrrolidine]-2,3,4-tricarboxylate **(17a):** yellow powder, m. p. 182–184°C, yield 97%. IR (KBr) (ν_{max}/cm^{-1}): 3,443, 1738, 1,735, 1,697, 1,656, 1,578, 1,487, and 1,298 cm^{-1}. ^{1}H NMR (500 MHz, $CDCl_3$): δ 1.05 (3 H, s, Me), 1.10 (3 H, s, Me), 1.25 (3 H, t, ^3J = 7.4 Hz, Me), 2.36 (3 H, s, NMe), 2.76 (3 H, s, NMe), 2.83 (1 H, d, ^2J = 6.2 Hz, CH), 3.07 (1 H, d, ^2J = 6.2 Hz, CH), 3.65 (1 H, s, CH), 3.84 (3 H, s, MeO), 3.91 (3 H, s, MeO), 4.34 (2 H, q, ^3J = 7.4 Hz, CH_2O), 6.29 (1 H, s, CH), 7.08 (1 H, t, ^3J = 7.3 Hz, CH), 7.23 (1 H, d, ^3J = 8.6 Hz, CH), 7.38 (1 H, t, ^3J = 7.6 Hz, CH), 7.46 (1 H, d, ^3J = 7.6 Hz, CH), 10.24 (1 H, s, NH), and 10.86 (1 H, s, NH) ppm. ^{13}C NMR (125.7 MHz, $CDCl_3$): δ 14.25, 25.55, 25.95, 38.20, 40.51, 52.32, 52.49, 60.81, 63.18, 65.19, 76.03, 101.03, 115.66, 122.78, 122.92, 123.12, 124.23, 126.82, 128.54, 133.61, 133.63, 137.22, 137.23, 141.65, 144.27, 149.74, 162.30, 164.42, 165.83, 166.63, and 172.11 ppm. MS, *m/z* (%): 617 (M$^+$, 10), 147 (68), and 31 (100). Anal. Calcd for $C_{32}H_{33}N_5O_8$ (615.64): C, 62.43; H, 5.40; N, 11.38; Found: C, 62.52; H, 5.53; N, 11.46%.

Valuation of the antioxidant property via DPPH

As mentioned previously in this research, the antioxidant property of some synthesized spiropyridoindolepyrrolidines

such as **7a-7d** was investigated using the DPPH free radical utilizing Shimada et al.'s (1992) procedures. According to the Shimada method, the concentration of spiropyridoindolepyrrolidines **7a-7d** were selected 200–1,000 ppm, in which methanolic solution of DPPH (1 mmol/L) in equivalent volume was added to spiropyridoindolepyrrolidines solution. The new mixture was mixed at room temperature and after 30 min placed in a dark room that absorbance of mixture reached to 517 nm. For comparing the antioxidant activity of synthesized spiropyridoindolepyrrolidine **7a-7d,** butylated hydroxytoluene (BHT) and 2-tertbutylhydroquinone (TBHQ) were utilized and instead of synthesized compounds, methanol (3 ml) was used. For measuring the percentage of inhibition of the DPPH radical trapping experiment, the Yen and Duh (1994) equation was used.

FRAP process promoted evaluation of the spiropyridoindolpyrrolidine antioxidant activity

Another way for the consideration of spiropyridoindolepyrrolidine antioxidant property is by using the FRAP process that measures the amounts of iron (III) reducing by synthesized spiropyridoindolepyrrolidines **7a-7d,** employing the Yildirim et al. procedure (Yildirim et al., 2001). In this experiment, the spiropyridoindolepyrrolidine solution (1 ml), potassium ferricyanide (2.6 ml), and phosphate buffer (2.6 ml) was used for the evaluation of antioxidant activity according to Yildirim et al.'s procedure. The temperature of the mixture was kept at 55°C for 35 min and then trichloroacetic acid (2.5 ml) was added and to the new mixture was stirred for 10 min. Finally, the absorbance of $FeCl_3$ (0.6 ml) and supernatant (2.5 ml) mixture in aqueous media (2.6 ml) as a sample was measured at 700 nm. As a result, compounds with a high reducing ability have high amount of absorbance. All computations were carried out three times for the confirmation of calculating. Running the SPSS software version 18.0 is a way to study of variance (ANOVA) for synthesized spiropyridoindolepyrrolidine data analyzing the approved samples and standard variation. Duncan multiple-range experiments were employed for separation with the important extent of 95% ($p < 0.05$).

Study of the antibacterial activity of the prepared spiropyridoindolepyrrolidine

For this investigation, Persian-type culture collection (PTCC) of Gram-positive and Gram-negative bacteria was prepared in Tehran, Iran, and for this reason, the disk diffusion procedure was utilized. For performing the evaluation of spiropyridoindolepyrrolidine antimicrobial ability, two types of bacterial concentration were similar to McFarland Standard No. 0.5 and were cultured for 16–24 h at 37 C. Two standard drugs such as streptomycin and gentamicin that killed bacteria were utilized. The suspension of bacteria was prepared with a sterile swab cultured on Mueller Hinton agar consistent with McFarland standard No. 0.5 (1.5 × 108 CFU/ml). Then, for the consideration of antibacterial property, spiropyridoindolepyrrolidine (25 μg/ml) was added on sterile blank disks, and the ready sample was placed for 24 h at 37 C in an incubator. The diameter of the inhibition zone was measured and compared to the standard sample.

The $Ag/Fe_3O_4/CdO$@MWCNT MNC application in the reduction of 4-NP

For this purpose, the mixture of $Ag/Fe_3O_4/CdO$@MWCNT MNCs (0.005 g) and 4-nitrophenol solution (25 ml, 2.5 mM) was stirred for 2 min at room temperature in the beaker, and the newly produced $NaBH_4$ (25 ml, 0.25 M) was added to the previous mixture as a reducing agent, which could remove the pollutant in the presence of a catalyst. After adding the aqueous $NaBH_4$ to the first mixture, the solution color varied from pale yellow to lemon color. The stirring of the mixture was continued till the mixture became colorless. When the reaction mixture became colorless, for measuring the UV–Vis absorption, 1 ml of the solution was diluted to 25 ml at certain times. The concentration of 4-nitrophenol varied between 200 and 700 nm at room temperature, and it was checked by the UV–Vis absorption spectra. The main point in the catalyst is reusability of it in the same reactions. For the confirmation of this point, the catalyst was removed from the reaction mixture and washed with ethanol and finally dried for reusing in the same reaction.

6 Theoretical simulations

Computational details

Theoretical studies were carried out by the Gaussian 09 package (Frisch et al., 2009). The electronic structure and geometries, Mulliken atomic charges, and vibrational frequencies of 6a-6d compounds were computed within the density functional theory DFT/B_3LYP method with 6–311++G** basis set. The global reactivity descriptors such as ionization energy (I), electron affinity (A), chemical potential (μ), chemical hardness (η), molecular electrophilicity (w), and chemical softness were computed from the energies of HOMO and LUMO using equations (1)-(6) (Umadevi and Lalitha, 2012), and the values reactivity descriptors were obtained using Multiwfn 3.7 code Lu et al., 2012). For a good agreement between theoretical and

experimental data, the calculated frequencies were scaled using the Pulay scaled quantum mechanical force field methodology.

$$I = -E_{HOMO}, \quad (1)$$

$$A = -E_{LUMO}, \quad (2)$$

$$\mu = (E_{LUMO} + E_{HOMO})/2, \quad (3)$$

$$\eta = (E_{LUMO} - E_{HOMO})/2, \quad (4)$$

$$S = 1/\eta, \quad (5)$$

$$\omega = \mu^2/2\eta. \quad (6)$$

Data availability statement

The original contributions presented in the study are included in the article/Supplementary Material. Further inquiries can be directed to the corresponding author.

Author contributions

The role of ZH in this article is performing synthesis of compounds, investigation, and writing the manuscript. The role of MM in this article is performing and writing the theoretical section. The role of FS-F in this article is the synthesis of compounds and performing analysis for synthesized compounds.

Acknowledgments

The authors thank Islamic Azad University and Vali-e-Asr University of Rafsanjan.

Conflict of interest

The authors declare no conflict of interest, financial or otherwise.

Publisher's note

All claims expressed in this article are solely those of the authors and do not necessarily represent those of their affiliated organizations, or those of the publisher, the editors, and the reviewers. Any product that may be evaluated in this article, or claim that may be made by its manufacturer, is not guaranteed or endorsed by the publisher.

Supplementary material

The Supplementary Material for this article can be found online at: https://www.frontiersin.org/articles/10.3389/fchem.2022.949205/full#supplementary-material

References

Abdolmohammadi, S. (2013). Study of the catalytic activity of Zr(HPO4)2 in the synthesis of hexahydroquinoline derivatives under solvent-free conditions. *Z. für Naturforsch. B* 68, 195–200. doi:10.5560/znb.2013-2237

Abdolmohammadi, S. (2014b). α-ZrP: A highly efficient catalyst for solvent-free synthesis of pyrimido[5', 4':5, 6]pyrido[2, 3-d]pyrimidinetetraone and 4-arylacridinedione derivatives. *Lett. Org. Chem.* 11, 465–469. doi:10.2174/15701786111666140124002242

Abdolmohammadi, S., Balalaie, S., Barari, M., and Rominger, F. (2013). Three-Component green reaction of arylaldehydes, 6-amino-1, 3-dimethyluracil and active methylene compounds catalyzed by Zr(HSO4)4 under solvent-free conditions. *Comb. Chem. High. Throughput Screen.* 16, 150–159. doi:10.2174/1386207311316020009

Abdolmohammadi, S., and Hossaini, Z. S. (2019). Fe3O4 MNPs as a green catalyst for syntheses of functionalized [1, 3]-oxazole and 1H-pyrrolo-[1, 3]-oxazole derivatives and evaluation of their antioxidant activity. *Mol. Divers.* 23, 885–896. doi:10.1007/s11030-019-09916-9

Abdolmohammadi, S., Hossaini, Z. S., and Poor Heravi, R. (2022). PANI-Fe3O4@ZnO nanocomposite as magnetically recoverable organometallic nanocatalyst promoted synthesis of new azo chromene dyes and evaluation of their antioxidant and antimicrobial activities. *Mol. Divers.* 26, 1983–1993. In press. doi:10.1007/s11030-021-10309-0

Abdolmohammadi, S., Mirza, B., and Vessally, E. (2019). Immobilized TiO2 nanoparticles on carbon nanotubes: An efficient heterogeneous catalyst for the synthesis of chromeno[b]pyridine derivatives under ultrasonic irradiation. *RSC Adv.* 9, 41868–41876. doi:10.1039/c9ra09031b

Abdolmohammadi, S., Pirelahi, H., Balalaie, F., and Balalaie, S. (2010). Efficient synthesis of dihydrochromeno[4, 3-b]chromenone derivatives in aqueous media. *Hetrocyclic Commun.* 16, 13–20.

Abdolmohammadi, S., Rasouli Nasrabadi, S. R., Dabiri, M. R., and Banihashemi Jozdani, S. M. (2020a). TiO2 nanoparticles immobilized on carbon nanotubes: An efficient heterogeneous catalyst in cyclocondensation reaction of isatins with malononitrile and 4-hydroxycoumarin or 3, 4-methylenedioxyphenol under mild reaction conditions. *Appl. Organomet. Chem.* 34, e5462. doi:10.1002/aoc.5462

Abdolmohammadi, S., Shariati, S., Elmi Fard, N., and Samani, A. (2020b). Aqueous-Mediated green synthesis of novel spiro[indole-quinazoline] derivatives using kit-6 mesoporous silica coated Fe 3 O 4 nanoparticles as catalyst. *J. Heterocycl. Chem.* 57, 2729–2737. doi:10.1002/jhet.3981

Abdolmohammadi, S., Shariati, S., and Mirza, B. (2021). Ultrasound promoted and Kit-6 mesoporous silica-supported Fe $_3$ O $_4$ magnetic nanoparticles catalyzed cyclocondensation reaction of 4-hydroxycoumarin, 3, 4-methylenedioxyphenol, and aromatic aldehydes. *Appl. Organomet. Chem.* 35, e6117. doi:10.1002/aoc.6117

Abdolmohammadi, S. (2014a). Silica supported Zr(HSO_4)4 catalysed solvent-free synthesis of [1]benzopyrano[4, 3-b] [1]benzopyran-6-ones and xanthenones. *Lett. Org. Chem.* 11, 350–355. doi:10.2174/15701786106661312122317O9

Abdolmohammadi, S. (2018). TiO2 NPs-coated carbone nanotubes as a green and efficient catalyst for the synthesis of [1]benzopyrano[b] [1]benzopyranones and xanthenols in water. *Comb. Chem. High. Throughput Screen.* 21, 594–601. doi:10.2174/1386207321666181018164739

Aboonajmi, J., Panahi, F., and Sharghi, H. (2021). One-pot multicomponent coupling reaction of catechols, benzyl alcohols/benzyl methyl ethers, and ammonium acetate toward synthesis of benzoxazoles. *ACS Omega* 6, 22395–22399. doi:10.1021/acsomega.1c03207

Ahmadi, F., Kadivar, M., and Shahedi, M. (2007). Antioxidant activity of Kelussia odoratissima Mozaff. in model and food systems. *Food Chem. x.* 105, 57–64. doi:10.1016/j.foodchem.2007.03.056

Amir, M., Javed, S. A., and Kumar, H. (2007). Pyrimidine as antiinflammatory agent: A review. *Indian J. Pharm. Sci.* 69, 337–343. doi:10.4103/0250-474x.34540

Azizi, Z., Ghambarian, M., Rezaei, M. A., and Ghashghaee, M. (2015). Saturated N, X-heterocyclic carbenes (X= N, O, S, P, Si, C, and B): Stability, nucleophilicity, and basicity. *Aust. J. Chem.* 68, 1438–1445. doi:10.1071/ch14715

Babizhayev, M. A., Deyev, A. I., Yermakovea, V. N., Brikman, I. V., and Bours, J. (2004). Lipid peroxidation and cataracts: N-Acetylcarnosine as a therapeutic tool to

manage age-related cataracts in human and in canine eyes. *Drugs R. D.* 5, 125–139. doi:10.2165/00126839-200405030-00001

Balar, M., Azizi, Z., and Ghashghaee, M. (2016). Theoretical identification of structural heterogeneities of divalent nickel active sites in NiMCM-41 nanoporous catalysts. *J. Nanostructure Chem.* 6, 365–372. doi:10.1007/s40097-016-0208-z

Bidchol, A. M., Wilfred, A., Abhijna, P., and Harish, R. (2011). Free radical scavenging activity of aqueous and ethanolic extract of *Brassica oleracea* L. Var. italica. *Food bioproc. Tech.* 4, 1137–1143. doi:10.1007/s11947-009-0196-9

Chaghari-Farahani, F., Abdolmohammadi, S., and Kia-Kojoori, R. (2020). A PANI-Fe_3O_4@ZnO nanocomposite: A magnetically separable and applicable catalyst for the synthesis of chromeno-pyrido[*d*]pyrimidine derivatives. *RSC Adv.* 10, 15614–15621. doi:10.1039/d0ra01978j

Chen, X., Mao, J., Liu, C., Chen, C., Cao, H., and Yu, L. (2020). An unexpected generation of magnetically separable Se/Fe3O4 for catalytic degradation of polyene contaminants with molecular oxygen. *Chin. Chem. Lett.* 31, 3205–3208. doi:10.1016/j.cclet.2020.07.031

Dastan, A., Kulkarnia, A., and Torok, B. (2012). Environmentally benign synthesis of heterocyclic compounds by combined microwave-assisted heterogeneous catalytic approaches†. *Green Chem.* 14, 17–37. doi:10.1039/c1gc15837f

Desai, N., Trivedi, A., Pandit, U., Dodiya, A., Rao, V. K., and Desai, P. (2016). Hybrid bioactive heterocycles as potential antimicrobial agents: A review. *Mini. Rev. Med. Chem.* 16, 1500–1526. doi:10.2174/1389557516666160609075620

Djurišić, A. B., Chen, X., Leung, Y. H., and Man, A. (2012). ZnO nanostructures: Growth, properties and applications. *J. Mat. Chem.* 22, 6526–6535. doi:10.1039/c2jm15548f

Ebrahimi, A., Habibi, S. M., Sanati, A., and Mohammadi, M. (2008). A comparison of C–C rotational barrier in [2] staffane, [2] tetrahedrane and ethane. *Chem. Phys. Lett.* 466, 32–36. doi:10.1016/j.cplett.2008.10.037

Ezzatzadeh, E., Farjam, M. H., and Rustaiyan, A. (2012). Comparative evaluation of antioxidant and antimicrobial activity of crude extract and secondary metabolites isolated from Artemisia kulbadica. *Asian Pac. J. Trop. Dis.* 2, S431–S434. doi:10.1016/s2222-1808(12)60198-4

Ezzatzadeh, E., and Hossaini, Z. S. (2019). Green synthesis and antioxidant activity of novel series of benzofurans from euparin extracted of Petasites hybridus. *Nat. Prod. Res.* 33, 1617–1623. doi:10.1080/14786419.2018.1428598

Fakheri-Vayeghan, S., Abdolmohammadi, S., and Kia-Kojoori, R. (2018). An expedient synthesis of 6-amino-5-[(4-hydroxy-2-oxo-2H-chromen-3-yl)(aryl) methyl]-1, 3-dimethyl-2, 4, 6(1H, 3H)-pyrimidinedione derivatives using Fe3O4@TiO2 nanocomposite as an efficient, magnetically separable, and reusable catalyst. *Z. für Naturforsch. B* 73, 545–551. doi:10.1515/znb-2018-0030

Foresman, J. B., and Frisch, A. E. (1996). *Exploring chemistry with electronic structure methods*. 2nd ed. Pittsburgh, PA: Gaussian, Inc.

Fouad, M. M., El-Bendary, E. R., Suddek, G. M., Shehata, I. A., and El-Kerdawy, M. M. (2018). Synthesis and *in vitro* antitumor evaluation of some new thiophenes and thieno[2, 3-d]pyrimidine derivatives. *Bioorg. Chem.* 81, 587–598. doi:10.1016/j.bioorg.2018.09.022

Frisch, M. J., Trucks, G. W., Schlegel, H. B., Scuseria, G. E., Robb, M. A., Cheeseman, J. R., et al. (2009). *Gaussian 09 (revision A.02)*. Wallingford, CT: Gaussian.

Ghambarian, M., Azizi, Z., and Ghashghaee, M. (2016). Diversity of monomeric dioxo chromium species in Cr/silicalite-2 catalysts: A hybrid density functional study. *Comput. Mater. Sci.* 118, 147–154. doi:10.1016/j.commatsci.2016.03.009

Ghambarian, M., Azizi, Z., and Ghashghaee, M. (2020). Remarkable improvement in phosgene detection with a defect-engineered phosphorene sensor: First-principles calculations. *Phys. Chem. Chem. Phys.* 22, 9677–9684.

Ghambarian, M., Ghashghaee, M., and Azizi, Z. (2017). Coordination and siting of Cu+ ion adsorbed into silicalite-2 porous structure: A density functional theory study. *Phys. Chem. Res.* 5, 135–152.

Ghashghaee, M., Azizi, Z., and Ghambarian, M. (2020b). Adsorption of iron (II, III) cations on pristine heptazine and triazine polymeric carbon nitride quantum dots of buckled and planar structures: Theoretical insights. *Adsorption* 26, 429–442. doi:10.1007/s10450-019-00197-0

Ghashghaee, M., Azizi, Z., and Ghambarian, M. (2020a). Substitutional doping of black phosphorene with boron, nitrogen, and arsenic for sulfur trioxide detection: A theoretical perspective. *J. Sulfur Chem.* 41, 399–420. doi:10.1080/17415993.2020.1752692

Ghashghaee, M., Ghambarian, M., and Azizi, Z. (2019). Molecular-level insights into furfural hydrogenation intermediates over single-atomic Cu catalysts on magnesia and silica nanoclusters. *Mol. Simul.* 45, 154–163. doi:10.1080/08927022.2018.1547820

Ghashghaee, M., and Ghambarian, M. (2020). Defect engineering and zinc oxide doping of black phosphorene for nitrogen dioxide capture and detection: Quantum-chemical calculations. *Appl. Surf. Sci.* 523, 146527. doi:10.1016/j.apsusc.2020.146527

Ghavidel, H., Mirza, B., and Soleimani-Amiri, S. (2021). A novel, efficient, and recoverable basic Fe3O4@C nano-catalyst for green synthesis of 4H-chromenes in water via one-pot three component reactions. *Polycycl. Aromat. Compd.* 41, 604–625. doi:10.1080/10406638.2019.1607413

Goel, A., Agarwal, N., Singh, F. V., Sharon, A., Tiwari, P., Dixit, M., et al. (2004). Antihyperglycemic activity of 2-methyl-3, 4, 5-triaryl-1 H -pyrroles in SLM and STZ models. *Bioorg. Med. Chem. Lett.* 14, 1089–1092. doi:10.1016/j.bmcl.2004.01.009

Guo, Z., Liu, B., Zhang, Q., Deng, W., Wang, Y., and Yang, Y. (2004). Recent advances in heterogeneous selective oxidation catalysis for sustainable chemistry. *Chem. Soc. Rev.* 43, 3480–3524. doi:10.1039/c3cs60282f

Hajinasiri, R., Hossaini, Z. S., and Sheikholeslami-Farahani, F. (2015). ZnO-nanorods as the catalyst for the synthesis of 1, 3-thiazole derivatives via multicomponent reactions. *Comb. Chem. High. Throughput Screen.* 18, 42–47. doi:10.2174/1386207317666141203123133

Halliwell, B. (1999). Antioxidant defence mechanisms: From the beginning to the end (of the beginning). *Free Radic. Res.* 31, 261–272. doi:10.1080/10715769900300841

Hassanabadi, A., and Khandan-Barani, K. (2013). Three-component and one-pot reaction between phenacyl bromide and primary amines in the presence of carbon disulfide. *J. Chem. Res.* 37, 71–72. doi:10.3184/174751912x13568926198645

Hekmatara, S. H., Mohammadi, M., and Haghani, M. (2019). Novel water-soluble, copolymer capped zinc oxide nanorods with high photocatalytic activity for degradation of organic pollutants from water. *Chem. Phys. Lett.* 730, 345–353. doi:10.1016/j.cplett.2019.05.046

Herrera, R. P., and Marqués-López, E. (2015). *Multicomponent reactions: Concepts and applications for design and synthesis*. Hoboken: Wiley.

Ibarra, I. A., Islas-Jácome, A., and González-Zamora, E. (2018). Synthesis of polyheterocycles*via*multicomponent reactions. *Org. Biomol. Chem.* 16, 1402–1418. doi:10.1039/c7ob02305g

Jabłonska, M., and Palkovits, R. (2016). Nitrogen oxide removal over hydrotalcite-derived mixed metal oxides. *Catal. Sci. Technol.* 6, 49–72. doi:10.1039/c5cy00646e

Janitabar-Darzi, S., and Abdolmohammadi, S. (2019). TiO_2-SiO_2 nanocomposite as a highly efficient catalyst for the solvent-free cyclocondensation reaction of isatins, cyclohexanones, and urea. *Z. für Naturforsch. B* 74, 559–564. doi:10.1515/znb-2019-0059

Kalantari, E., Khalilzadeh, M. A., Zareyee, D., and Shokouhimehr, M. (2020). Catalytic degradation of organic dyes using green synthesized Fe3O4-cellulose-copper nanocomposites. *J. Mol. Struct.* 1218, 128488. doi:10.1016/j.molstruc.2020.128488

Kalaria, P. N., Karad, S. C., and Raval, D. K. (2018). A review on diverse heterocyclic compounds as the privileged scaffolds in antimalarial drug discovery. *Eur. J. Med. Chem.* 158, 917–936. doi:10.1016/j.ejmech.2018.08.040

Kassaee, M. Z., Ghambarian, M., and Musavi, S. M. (2008). Halogen switching of azacarbenes C2NH ground states at *ab initio* and DFT levels. *Heteroat. Chem.* 19, 377–388. doi:10.1002/hc.20442

Kassaee, M. Z., Hossaini, Z. S., Haerizade, B. N., and Sayyed-Alangi, S. Z. (2004). *Ab initio* study of steric effects due to dialkyl substitutions on H2C3 isomers. *J. Mol. Struct. THEOCHEM* 681, 129–135. doi:10.1016/j.theochem.2004.05.014

Kassaee, M. Z., Momeni, M. R., Shakib, F. A., Ghambarian, M., and Musavi, S. M. (2010). Novel α-spirocyclic (alkyl)(amino) carbenes at the theoretical crossroad of flexibility and rigidity. *Struct. Chem.* 21, 593–598. doi:10.1007/s11224-010-9585-y

Khalilian, S., Abdolmohammadi, S., and Nematolahi, F. (2017). An eco-friendly and highly efficient synthesis of pyrimidinones using a TiO2-CNTs nanocomposite catalyst. *Lett. Org. Chem.* 14, 361–367. doi:10.2174/1570178614666170321113926

Khalilzadeh, M. A., Hosseini, S., Rad, A. S., and Venditti, R. A. (2021). Synthesis of grafted nanofibrillated cellulose-based hydrogel and study of its thermodynamic, kinetic, and electronic properties. *J. Agric. Food Chem.* 68, 8710–8719. doi:10.1021/acs.jafc.0c03500

Khandan-Barani, K., Maghsoodlou, M. T., Habibi-Khorasani, S. M., Hazeri, N., and Sajadikhah, S. S. (2011). Three-component reaction between alkyl (aryl) isocyanides and dialkyl acetylenedicarboxylates in the presence of ethyl trifluoroacetate. *J. Chem. Res.* 35, 231–233. doi:10.3184/174751911x13025338429293

Khandan-Barani, K., Maghsoodlou, M. T., Hassanabadi, A., Hosseini-Tabatabaei, M. R., Saffari, J., and Kangani, M. (2015). Synthesis of maleate derivatives in isocyanide-base MCRs: Reaction of 2-mercaptobenzoxazole with alkyl isocyanides

and dialkyl acetylenedicarboxylates. *Res. Chem. Intermed.* 41, 3011–3016. doi:10.1007/s11164-013-1409-4

Khattab, T. A., and Rehan, M. A. (2018). Egypt. *J. Chem.* 61, 989–1018.

Koohi, M., Soleimani Amiri, S., and Shariati, M. (2017). Silicon impacts on structure, stability and aromaticity of C20-nSin heterofullerenes (n= 1–10): A density functional perspective. *J. Mol. Struct.* 1127, 522–531. doi:10.1016/j.molstruc.2016.08.012

Lamberth, C., and Dinges, J. (2012). *Bioactive heterocyclic compound classes: Agrochemicals*. Wiley-VCH Verlag GmbH & Co, KGaA.

Lashkari, M., Maghsoodlou, M. T., Hazeri, N., Habibi-Khorassani, S. M., Akbarzadeh Torbati, N., García-Granda, S., et al. (2015). A novel route for the diastereoselective synthesis of dispiro[tetrahydroquinoline-bis(2, 2-dimethyl[1, 3] dioxane-4, 6-dione)] derivatives via a one-pot domino multicomponent reaction of arylamines, aromatic aldehydes, and meldrum's acid. *J. Heterocycl. Chem.* 52 (3), 873–879. doi:10.1002/jhet.1984

Li, W., Zhao, S. J., Gao, F., Lv, Z. S., Tu, J. Y., and Xu, Z. (2018). Synthesis and *in vitro* anti-tumor, anti-mycobacterial and anti-HIV activities of diethylene-glycol-tethered bis-isatin derivatives. *ChemistrySelect* 3, 10250–10254. doi:10.1002/slct.201802185

Lin-Bing, S., Xiao-Qin, L., and Hong-Cai, Z. (2015). *Chem. Soc. Rev.* 44, 5092–5147.

Liu, L., and Meydani, M. (2002). Combined vitamin C and E supplementation retards early progression of arteriosclerosis in heart transplant patients. *Nutr. Rev.* 60, 368–371. doi:10.1301/00296640260385810

Lu, Tian, and Chen, Feiwu (2012). Multiwfn: A multifunctional wavefunction analyzer. *J. Comput. Chem.* 33, 580–592. doi:10.1002/jcc.22885

Maghsoodlou, M. T., Hazeri, N., Khandan-Barani, K., Habibi-Khorasani, S. M., and Abedi, A. (2014). Synthesis of 1-(Cyclohexylamino)-2-(aryl) pyrrolo [1, 2-a] quinoline-3-carbonitrile derivatives using a mild, four-component reaction. *J. Heterocycl. Chem.* 51, E152–E155. doi:10.1002/jhet.1913

Martins, P., Jesus, J., Santos, S., Raposo, L. R., Roma-Rodrigues, C., Baptista, P. V., et al. (2015). Heterocyclic anticancer compounds: Recent advances and the paradigm shift towards the use of nanomedicine's tool box. *Molecules* 20, 16852–16891. doi:10.3390/molecules200916852

Masoodi, H. R., Bagheri, S., Mohammadi, M., Zakarianezhad, M., and Makiabadi, B. (2013). The influence of cation–π and anion–π interactions on some NMR data of s-triazine HF hydrogen bonding: A theoretical study. *Chem. Phys. Lett.* 588, 31–36. doi:10.1016/j.cplett.2013.09.067

Mebi, A. C. (2011). DFT study on structure, electronic properties, and reactivity of Cis¬Isomers of [(NC5H4¬S) 2Fe (CO) 2]. *J. Chem. Sci. (Bangalore).* 123, 727–731. doi:10.1007/s12039-011-0131-2

Mohammadi, M., Hekmatara, S. H., Moghaddam, R. S., and Darehkordi, A. (2019). Preparation and optimization photocatalytic activity of polymer-grafted Ag@ AgO core-shell quantum dots. *Environ. Sci. Pollut. Res.* 26, 13401–13409. doi:10.1007/s11356-019-04685-2

Mousavi, M. R., Aboonajmi, J., Maghsoodlou, M. T., and Hazeri, N. (2014). Y(NO3)3·4H2O-assisted three-component synthesis of polysubstituted tetrahydropyridines. *J. Chem. Res.* 38, 76–79. doi:10.3184/174751914x13890195583234

Mulliken, R. S. (1955). Electronic population analysis on LCAO–MO molecular wave functions. I. *J. Chem. Phys.* 23, 1833–1840. doi:10.1063/1.1740588

Rabiei, A., Abdolmohammadi, S., and Shafaei, F. (2017). A green approach for an efficient preparation of 2, 4-diamino-6-aryl-5-pyrimidinecarbonitriles using a TiO2/SiO2 nanocomposite catalyst under solvent-free conditions. *Z. für Naturforsch. B* 72, 241–247. doi:10.1515/znb-2016-0219

Rajendran, S. P., and Sengodan, K. (2017). Synthesis and characterization of zinc oxide and iron oxide nanoparticles using *Sesbania grandiflora* leaf extract as reducing agent. *J. Nanosci.*, 1–7. doi:10.1155/2017/8348507

Rustaiyan, A., and Ezzatzadeh, E. (2011). Sesquiterpene lactones and penta methoxylated flavone from Artemisia kulbadica. *Asian J. Chem.* 23, 1774–1776.

Rustaiyan, A., Masoudi, S., Ezzatzadeh, E., Akhlaghi, H., and Aboli, J. (2011). Composition of the aerial part, flower, leaf and stem oils of eremostachys macrophylla montbr. & auch. And eremostachys labiosa bunge. From Iran. *J. Essent. Oil Bear. Plants* 14, 84–88. doi:10.1080/0972060x.2011.10643904

Sabbaghan, M., Yavari, I., and Hossaini, Z. S. (2010). Synthesis of functionalized chromenes from meldrum's acid, 4-hydroxycoumarin, and ketones or aldehydes. *Comb. Chem. High. Throughput Screen.* 13, 813–817. doi:10.2174/138620710792927358

Sahay, R., Sundaramurthy, J., Suresh Kumar, P., Thavasi, V., Mhaisalkar, S. G., and Ramakrishna, S. (2012). Synthesis and characterization of CuO nanofibers, and investigation for its suitability as blocking layer in ZnO NPs based dye sensitized solar cell and as photocatalyst in organic dye degradation. *J. Solid State Chem.* 186, 261–267. doi:10.1016/j.jssc.2011.12.013

Salehi Borban, S., Gharachorloo, M., and Zamani Hargalani, F. (2017). Check Amount of heavy metals in muscle and fish oil Rutilus frisii kutum, Clupeonella cultriventris and Liza saliens. *J. Food Technol. Nutr.* 6, 75–104.

Samani, A., Abdolmohammadi, S., and Otaredi-Kashani, A. (2018). A green synthesis of xanthenone derivatives in aqueous media using TiO2-CNTs nanocomposite as an eco-friendly and Re-usable catalyst. *Comb. Chem. High. Throughput Screen.* 21, 111–116. doi:10.2174/1386207321666180219151705

Saundane, A. R., and Nandibeoor, M. K. (2015). Synthesis, characterization, and biological evaluation of Schiff bases containing indole moiety and their derivatives. *Monatsh. Chem.* 146, 1751–1761. doi:10.1007/s00706-015-1440-9

Seifi Mansour, S., Ezzatzadeh, E., and Safarkar, R. (2019). *In vitro* evaluation of its antimicrobial effect of the synthesized Fe3O4 nanoparticles using Persea Americana extract as a green approach on two standard strains. *Asian J. Green Chem.* 3, 353–365.

Shafaei, F., Babaei, S. E., Shahvelayati, A. S., and Honarmand Janatabadi, F. (2020). Biosynthesis of Fe3O4-magnetic nanoparticles using clover leaf aqueous extract: Green synthesis of 1, 3-benzoxazole derivatives. *J. Chin. Chem. Soc.* 67, 891–897. doi:10.1002/jccs.201800489

Shahvelayati, A. S., and Esmaeeli, Z. (2012). Efficient synthesis of S-dipeptidothiouracil derivatives via a one-pot, five-component reaction under ionic liquid condition. *J. Sulfur Chem.* 33, 319–325. doi:10.1080/17415993.2012.662982

Shahvelayati, A. S., Sabbaghan, M., and Banihashem, S. (2017). Sonochemically assisted synthesis of N-substituted pyrroles catalyzed by ZnO nanoparticles under solvent-free conditions. *Monatsh. Chem.* 148, 1123–1129. doi:10.1007/s00706-016-1904-6

Sharghi, H., Aboonajmi, J., Mozaffari, M., Doroodmand, M. M., and Aberi, M. (2018). Application and developing of iron-doped multi-walled carbon nanotubes (Fe/MWCNTs) as an efficient and reusable heterogeneous nanocatalyst in the synthesis of heterocyclic compounds. *Appl. Organomet. Chem.* 32, e4124. doi:10.1002/aoc.4124

Shi, J. (2013). On the synergetic catalytic effect in heterogeneous nanocomposite catalysts. *Chem. Rev.* 113, 2139–2181. doi:10.1021/cr3002752

Shimada, K., Fujikawa, K., Yahara, K., and Nakamura, T. (1992). Antioxidative properties of xanthan on the autoxidation of soybean oil in cyclodextrin emulsion. *J. Agric. Food Chem.* 40, 945–948. doi:10.1021/jf00018a005

Siddiqui, N., Andalip Bawa, S., Ali, R., Afzal, O., Akhtar, M. J., Azad, B., et al. (2011). Antidepressant potential of nitrogen-containing heterocyclic moieties: An updated review. *J. Pharm. Bioallied Sci.* 3, 194–212. doi:10.4103/0975-7406.80765

Sokolova, A. S., Yarovaya, O. I., Bormotov, N. I., Shishkina, L. N., and Salakhutdinov, N. F. (2018). Synthesis and antiviral activity of camphor-based 1, 3-thiazolidin-4-one and thiazole derivatives as *Orthopoxvirus*-reproduction inhibitors. *Medchemcomm* 9, 1746–1753. doi:10.1039/c8md00347e

Soleimani Amiri, S., Koohi, M., and Mirza, B. (2016). Characterizations of B and N heteroatoms as substitutional doping on structure, stability, and aromaticity of novel heterofullerenes evolved from the smallest fullerene cage C_{20}: A density functional theory perspective. *J. Phys. Org. Chem.* 29, 514–522. doi:10.1002/poc.3573

Soleimani-Amiri, S., Arabkhazaeli, M., Hossaini, Z. S., Afrashteh, S., and Eslami, A. A. (2018). Synthesis of chromene derivatives via three-component reaction of 4-hydroxycumarin catalyzed by magnetic Fe3O4 nanoparticles in water. *J. Heterocycl. Chem.* 55, 209–213. doi:10.1002/jhet.3028

Tietze, L. F., Bsasche, C., and Gericke, K. M. (2006). *Domino reactions in organic synthesis*. Weinheim: Wiley VCH.

Umadevi, P., and Lalitha, P. (2012). Synthesis and antimicrobial evaluation of amino substituted 1, 3, 4 oxo and thiadiazoles. *Int. J. Pharm. Pharm. Sci.* 4, 523–527.

Venkatesh, G., Govindaraju, M., Vennila, P., and Kamal, C. J. (2016). Molecular structure, vibrational spectral assignments (FT-IR and FT-Raman), NMR, NBO, HOMO–LUMO and NLO properties of 2-nitroacetophenone based on DFT calculations. *J. Theor. Comput. Chem.* 15, 1650007. doi:10.1142/s0219633616500073

Wachs, I. E. (2005). Recent conceptual advances in the catalysis science of mixed metal oxide catalytic materials. *Catal. Today* 100, 79–94. doi:10.1016/j.cattod.2004.12.019

Weber, L., Illgen, M., and Almstetter, M. (1999). Discovery of new multi component reactions with combinatorial methods. *Synlett* 3, 366–374. doi:10.1055/s-1999-2612

Yang, Y., Xu, B., He, J., Shi, J., Yu, L., and Fan, Y. (2020). Design and synthesis of Fe3O4@SiO2@mSiO2-Fe: A magnetically separable catalyst for selective oxidative

cracking reaction of styrene using air as partial oxidant. *Appl. Catal. A General* 590, 117353. doi:10.1016/j.apcata.2019.117353

Yang, Y., Xu, B., He, J., Shi, J., Yu, L., and Fan, Y. (2019). Magnetically separable mesoporous silica-supported palladium nanoparticle-catalyzed selective hydrogenation of naphthalene to tetralin. *Appl. Organomet. Chem.* 33, e5204. doi:10.1002/aoc.5204

Yavari, I., Sabbaghan, M., Porshamsian, K., Bagheri, M., Ali-Asgari, S., and Hossaini, Z. S. (2007). Efficient synthesis of alkyl 2-[2-(arylcarbonylimino)-3-aryl-4-oxo-1, 3-thiazolan-5-ylidene]-acetates. *Mol. Divers.* 11, 81–85. doi:10.1007/s11030-007-9061-9

Yavari, I., Seyfi, S., and Hossaini, Z. S. (2010). Formation of trialkyl quinoline-2, 3, 4-tricarboxylates by reaction of isatin, dialkyl acetylenedicarboxylates, and sodium O-alkyl carbonodithioates. *Tetrahedron Lett.* 51, 2193–2194. doi:10.1016/j.tetlet.2010.02.107

Yen, G. C., and Duh, P. D. (1994). Scavenging effect of methanolic extracts of peanut hulls on free-radical and active-oxygen species. *J. Agric. Food Chem.* 42, 629–632. doi:10.1021/jf00039a005

Yildirim, A., Mavi, A., and Kara, A. A. (2001). Determination of antioxidant and antimicrobial activities of *Rumex crispus* L. Extracts. *J. Agric. Food Chem.* 49, 4083–4089. doi:10.1021/jf0103572

Zare Davijani, N., Kia-Kojoori, R., Abdolmohammadi, S., and Sadegh-Samiei, S. (2022b). Employing of Fe3O4/CuO/ZnO@MWCNT MNCs in the solvent-free synthesis of new cyanopyrroloazepine derivatives and investigation of biological activity. *Mol. Divers.* 26, 2121–2134. In press. doi:10.1007/s11030-021-10319-y

Zare Davijani, N., Kia-Kojoori, R., Abdolmohammadi, S., and Sadegh-Samiei, S. (2022a). Ultrasonic-assisted synthesis of highly effective visible light Fe3O4/ZnO/PANI nanocomposite: Thoroughly kinetics and thermodynamic investigations on the Congo red dye decomposition. *J. Mol. Struct.* 1250, 131903. doi:10.1016/j.molstruc.2021.131903

Zhang, B.-T., Zheng, X., Li, H.-F., and Lin, J.-M. (2013). Application of carbon-based nanomaterials in sample preparation: A review. *Anal. Chim. Acta X.* 784, 1–17. doi:10.1016/j.aca.2013.03.054

Zhang, Q., Vigier, K. D. V., Royer, S., and Jerome, F. (2012). Deep eutectic solvents: Syntheses, properties and applications. *Chem. Soc. Rev.* 41, 7108–7146. doi:10.1039/c2cs35178a

Zhao, X., Chaudhry, S. T., and Mei, J. (2017). Heterocyclic building blocks for organic semiconductors. *Heterocycl. Chem. 21st Century a Tribute Alan Katritzky* 121, 133–171.

Zhao, Y., Xu, L., Yang, Ch., Chen, T., and Yu, L. (2019). *Appl. Organomet. Chem.* 33, e5112.

Zhi, S., Ma, X., and Zhang, W. (2019). Consecutive multicomponent reactions for the synthesis of complex molecules. *Org. Biomol. Chem.* 17, 7632–7650. doi:10.1039/c9ob00772e